

# An introduction to electrochemical methods for the functional analysis of metalloproteins

Christophe Léger \*

Laboratoire de Bioénergétique et Ingénierie des Protéines,  
Institut de Microbiologie de la Méditerranée, CNRS, AMU, Marseille, F  
[christophe.leger@imm.cnrs-mrs.fr](mailto:christophe.leger@imm.cnrs-mrs.fr), <http://bip.cnrs-mrs.fr/bip06>

February 7, 2012

We introduce electrochemistry of redox proteins and enzymes in the context of functional studies. We explain the fundamental concepts of electrochemistry only as far as they are important for understanding at a qualitative level the results that are presented. We have selected the latter to illustrate the variety of mechanistic information that can be gained from electrochemical investigations. We explain the most classical electrochemical experiments, but most results discussed herein were obtained using the configuration called “protein film voltammetry”, where the protein is adsorbed onto an electrode surface and electron transfer is direct. We shall not cover all aspects of Faradaic bioelectrochemistry: for example we do not discuss catalytic mediated electrochemistry, the characterisation of the electrode/protein interface in relation to the design of electrodes for immobilizing proteins, and applications in biotechnology (bio-fuel cells, bio-sensors, etc.).

Keywords: Redox enzymes, metalloenzymes, structure-function relationships, electrochemistry, direct electron transfer, protein film voltammetry, enzyme kinetics.

## Contents

|          |   |           |
|----------|---|-----------|
| <b>1</b> | <b>Introduction</b>   | <b>2</b>  |
| <b>2</b> | <b>Basics</b>   | <b>3</b>  |
| 2.1      | Redox thermodynamics: the Nernst equation . . . . .   | 3         |
| 2.2      | Reference potential and reference electrodes . . . . .  | 5         |
| 2.3      | The biological redox scale . . . . .  | 5         |
| 2.4      | Influence of coupled reactions (e.g. protonation or ligand binding) on reduction potentials . . . . . | 5         |
| 2.5      | Electron transfer (ET) kinetics . . . . .   | 8         |
| 2.6      | Kinetics of proton-coupled electron transfer: stepwise versus concerted mechanisms. . . . .           | 10        |
| <b>3</b> | <b>Electrochemistry under equilibrium conditions: potentiometric titrations</b>                       | <b>10</b> |
| <b>4</b> | <b>Dynamic electrochemistry</b>   | <b>11</b> |
| 4.1      | Distinction between equilibrium and dynamic electrochemistry . . . . .                                | 11        |
| 4.2      | Electrodes for electron transfer to/from proteins . . . . .   | 12        |

|          |  |           |
|----------|--|-----------|
| 4.3      | Electrochemical equipment . . . . .  | 13        |
| 4.4      | Vocab and conventions . . . . .  | 13        |
| 4.5      | The capacitive current . . . . .   | 13        |
| <b>5</b> | <b>Diffusion controlled Voltammetry</b>  | <b>14</b> |
| 5.1      | ...at stationary electrodes . . . . .  | 14        |
| 5.2      | ...at rotating electrodes . . . . .  | 16        |
| <b>6</b> | <b>“non-catalytic” protein film voltammetry (PFV)</b>                                  | <b>17</b> |
| 6.1      | Non-catalytic voltammetry at slow scan rates to measure reduction potentials . . . . . | 17        |
| 6.2      | Fast scan voltammetry to determine the rates of coupled reactions . . . . .            | 20        |
| <b>7</b> | <b>Catalytic protein film voltammetry and chronoamperometry</b>                        | <b>23</b> |
| 7.1      | Principle and general comments . . . . .   | 23        |
| 7.2      | Mass-transport controlled catalytic voltammetry . . . . .                              | 26        |
| 7.3      | Chronoamperometry to measure Michaelis and inhibition constants . . . . .              | 27        |
| 7.4      | Chronoamperometry to resolve rapid changes in activity . . . . .                       | 30        |
| 7.5      | Determining the reduction potentials of an active site bound to substrate . . . . .    | 31        |
| 7.6      | The effect of slow intramolecular electron transfer . . . . .                          | 33        |
| 7.7      | Slow interfacial electron transfer . . . . .   | 33        |
| 7.8      | Slow substrate binding . . . . .   | 33        |
| 7.9      | Slow, redox-driven (in)activation . . . . .  | 34        |
| <b>8</b> | <b>Softwares</b>   | <b>35</b> |
| <b>9</b> | <b>PFV Quiz</b>  | <b>36</b> |
| <b>A</b> | <b>Appendices</b>  | <b>36</b> |
| A.1      | Notations and abbreviations . . . . .  | 36        |
| A.2      | Derivation of eq. 9 . . . . .  | 37        |
|          | <b>References</b>  | <b>37</b> |

## 1 Introduction

Direct electron transfer to proteins (without the need for mediators) was first reported in the 1970's, opening the way for detailed studies of biological reactions, and electrochemical investigations of large redox enzymes are now common.

Determining reduction potentials is only one application of the method; in studies of redox proteins or small molecules, electrochemical techniques are used for learning not only about the thermodynamics but also the kinetics of chemical reactions that immediately precede or follow electron transfer (e.g. protonation or substrate binding). Using direct electrochemistry, the turnover rate of enzymes can also be measured with very high temporal resolution and potential control. This greatly broadens the possibilities of enzyme kinetics. This technique has indeed been used to study all aspects of catalysis: interfacial and intramolecular electron transfer, substrate diffusion along substrate channels, active site chemistry, mechanism of reaction with inhibitors, redox-driven (in)activation processes etc.

The proteins or enzymes that can be studied using direct electrochemistry have at least one surface-exposed redox center, which is the entry point for electrons from the electrode. The chance of success is greater when the protein of interest is small and hydrophilic, or, if it is an enzyme, when it has a large turnover rate. The amount of protein required depends on which method is used, but it can be as small as a few pmol for a series of experiments carried out with the same “film” of adsorbed proteins. The electrochemical equipment is particularly cheap (compared to many biophysical techniques) and available in most chemistry labs.

An extensive description of most of the electrochemical techniques will be found in refs [1, 2]. The physical aspects of electrochemistry, including hydrodynamics, are discussed in [3, 4]. Savéant provided a comprehensive discussion of voltammetric wave shapes under various conditions, with emphasis on the case where the electrocatalyst diffuses in solution [5]. Refs. [6, 7] are insightful textbooks on enzyme kinetics. There are many comprehensive reviews on the use of direct electrochemistry to probe the mechanism of redox proteins and enzymes [8–22]. Refs [16, 20] focus on hydrogenases. Armstrong and coworkers discuss in ref [17] the applications of redox enzymes in electrochemical devices. Ref [19] summarizes recent advances in the electrochemistry of *membrane-bound* redox enzymes. Lojou reviews in ref. [22] the strategies for connecting hydrogenases to electrodes.

## 2 Basics

### 2.1 Redox thermodynamics: the Nernst equation

Consider a reaction mixture containing the oxidised and reduced forms of two different species (1 and 2):



The free energy of the reaction ( $\Delta_r G$ , in units of J/mol) is given by

$$\Delta_r G = \Delta_r G^0 + RT \ln \frac{[\text{Red}_1][\text{Ox}_2]}{[\text{Ox}_1][\text{Red}_2]} \quad (2)$$

$R$  is the gas constant,  $T$  the absolute temperature and  $\Delta_r G^0$  is the (tabulated) standard free energy of the reaction (“Standard conditions” means that the activity of all constituents is unity, and the pressure equals one bar).

If equilibrium between the different species is reached,  $\Delta_r G = 0$ , and the ratio of concentrations (the reaction quotient) is linked to  $\Delta_r G^0$  by the relation:

$$K_{\text{eq}} = \frac{[\text{Red}_1]_{\text{eq}}[\text{Ox}_2]_{\text{eq}}}{[\text{Ox}_1]_{\text{eq}}[\text{Red}_2]_{\text{eq}}} = \exp\left(-\frac{\Delta_r G^0}{RT}\right) \quad (3)$$

Initially upon mixing  $\text{Ox}_1$  and  $\text{Red}_2$ , the concentrations of various species in the solution do not satisfy eq. (3), and  $\Delta_r G$  is non zero: the system is not at equilibrium. Thermodynamics predicts that reaction (1) will spontaneously proceed in the direction given by  $dG = \Delta_r G d\xi < 0$ , where  $d\xi$  is the change in the extent of reaction, until the reaction quotient equals  $K_{\text{eq}}$ .

During the reaction,  $\text{Red}_2$  is oxidised and gives electrons to  $\text{Ox}_1$ . The overall reaction can be

written as the sum of two “half-reactions”:



It is possible to measure the flux of electrons from  $\text{Red}_2$  to  $\text{Ox}_1$ , and therefore the *rate*  $d\xi/dt$  of the overall reaction, by placing the species in a two-compartment cell ( $\text{Ox}_1$  in one compartment and  $\text{Red}_2$  in the other). Place in each side an electrode at which the species can interact. When the two electrodes are connected together, a current flows, while the system evolves towards equilibrium. This current results from a potential difference between the two electrodes,  $V = E_2 - E_1$ , the value of which can be predicted applying the **Nernst equation** to each of the two electrodes.

$$E = E^0 + \frac{RT}{nF} \ln \frac{[\text{Ox}]}{[\text{Red}]} \quad (5)$$

$E^0$  is the standard reduction potential of the redox couple  $\text{Ox}/\text{Red}$ .  $F = 96500\text{C}$  is the Faraday constant.<sup>1</sup>

The electrode potential given by eq. 5 cannot be measured; only the difference between the potentials of two electrodes can. The potential difference between the electrodes in compartments 1 and 2 is:

$$V = E_2 - E_1 = E_2^0 - E_1^0 + \frac{RT}{nF} \ln \frac{[\text{Ox}_2][\text{Red}_1]}{[\text{Red}_2][\text{Ox}_1]} \quad (6)$$

The electrons are going to flow from the cell whose electrode potential is the lowest to the other until  $V$  and  $\Delta_r G$  are zero and the concentrations satisfy

$$K_{\text{eq}} = \frac{[\text{Red}_1]_{\text{eq}}[\text{Ox}_2]_{\text{eq}}}{[\text{Ox}_1]_{\text{eq}}[\text{Red}_2]_{\text{eq}}} = \exp\left(-\frac{nF}{RT}(E_2^0 - E_1^0)\right) \quad (7)$$

This is equivalent to eq. (3), since reduction potentials and free energies are linked by

$$\Delta_r G^0 = -nF(E_1^0 - E_2^0) \quad (8)$$

The Nernst equation can therefore be used to determine the direction in which a redox reaction will proceed spontaneously (eq. 6). Reaction (1) will proceed forward significantly ( $K_{\text{eq}}$  will be large) only if  $E_1^0 > E_2^0$ . If  $E_1^0$  is “high”,  $\text{Ox}_1$  is called a strong oxidant and  $\text{Red}_1$  is a weak reductant. But it may not be enough to compare standard reduction potentials, since the sign of  $\ln \frac{[\text{Ox}_2][\text{Red}_1]}{[\text{Ox}_1][\text{Red}_2]}$  in eq. (6) can change the sign of  $V$  (and  $\Delta_r G$ ) and thus the direction of the current flow. Also remember that thermodynamics predicts the direction but not the rate of the reaction: a “spontaneous” reaction might not happen because its rate is very small, in which case the equilibrium cannot be reached.

It makes more sense, in our opinion, to call  $E^0$  a standard *reduction* potential than a standard *redox* potential: the sign of  $\Delta_r G^0$  relates to a reaction proceeding in a certain direction, and the sign of a standard reduction potential (as defined in eq. 8) is what it is because the associated

<sup>1</sup>Note that the usage is to call  $E$  the “electrode potential”, but strictly speaking, it is the difference between the electrical potential of the metal electrode and the electrical potential of the solution adjacent to the metal,  $\Phi_M - \Phi_S$  [2]. The term  $\Phi_S$  cancels in an expression of the potential difference between two electrodes, as in eq. 6.

half-reaction is a reduction.

The reader should make sure he/she distinguishes between an *electrode* potential (the difference between two electrode potentials is measured using a voltmeter, it has unit of Volt, and relates to the free energy of the reaction, in units of J/mol) and a standard *reduction* potential (a thermodynamic property which is related by eq. 8 to a standard free energy of reaction). This should not be confused with the *electrochemical potential*, in units of J/mol, which is the equivalent of the partial free energy (or *chemical potential*) of a charged species with an additional term that accounts for the effect of the electric potential.

## 2.2 Reference potential and reference electrodes

If one is interested in studying only one half-reaction, it is convenient to make sure that the potential difference between the two electrodes reflects the potential of the electrode one is interested in. This can be done by using in the other compartment an electrode designed to have a constant potential: this is called a “*reference electrode*”.

The *Standard Hydrogen Electrode* (SHE) is one of these. It consists of a platinum electrode immersed in a pH=0 electrolyte under 1 bar of H<sub>2</sub>.

A real SHE is rarely practical. Instead one uses convenient reference electrodes such as:  
Hg/Hg<sub>2</sub>Cl<sub>2</sub>/KCl (Standard Calomel Electrode, SCE, E(SCE)=241mV *vs.* SHE.) This is the most commonly used reference electrode  
Hg/Hg<sub>2</sub>SO<sub>4</sub>/K<sub>2</sub>SO<sub>4</sub>, used when chloride ions must be avoided. E(SCE)=615mV *vs.* SHE.  
Ag/AgCl (E=200mV *vs.* SHE)

Since only potential differences can be measured, reduction potentials can only be reported against a certain reference electrode. The International Union of Pure and Applied Chemistry requires that this primary reference electrode be the SHE. All reduction potentials tabulated in the literature are (or should be) quoted versus the SHE. Therefore, by convention, the potential of the SHE is zero.

## 2.3 The biological redox scale

Because standard conditions (pH 0!) are not suitable for biological reactions, reduction potentials are usually stated for pH 7, and termed  $E^{0'}$  or  $E_{m,7}$ .

Figure 1 gives an idea of the range of reduction potentials spanned by biologically important redox cofactors and redox couples. It is important to realize that biological processes occur in water, and that the oxidation and reduction of water set the limits of the narrow range of relevant potentials. The reaction of a biological molecule under extreme (very oxidizing or very reducing) conditions may be interesting from the point of view of chemistry, but physiologically irrelevant.

## 2.4 Influence of coupled reactions (e.g. protonation or ligand binding) on reduction potentials

Redox reactions can be coupled to other chemical equilibria such as ligand binding (e.g. protons, substrate, inhibitor. . .) or conformational changes.

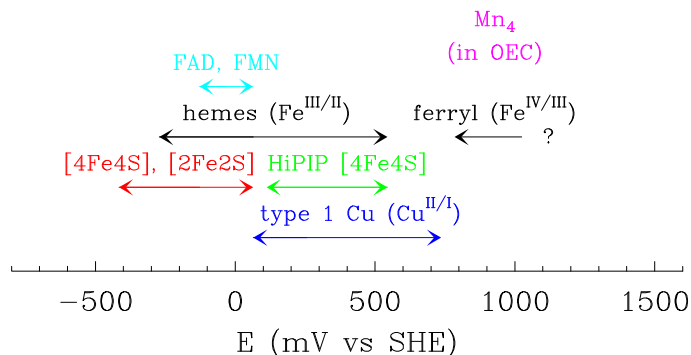


Figure 1: The biological redox scale at pH 7. “OEC” stands for the “oxygen evolving center” of Photosystem II.

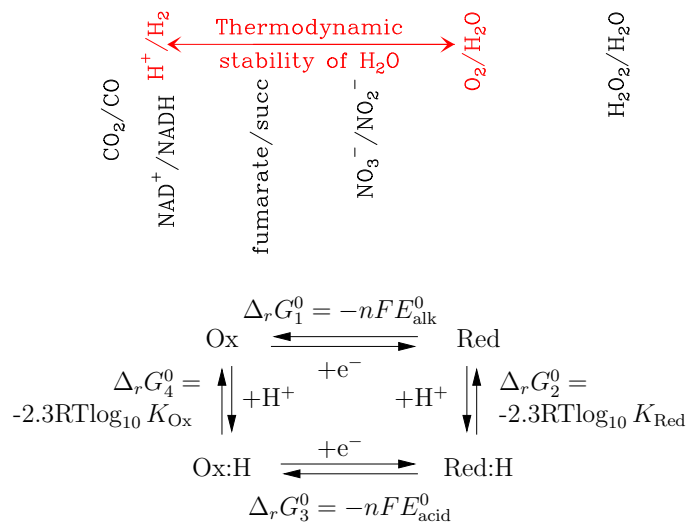


Figure 2: Square scheme for a protonation reaction coupled to a redox process.

A very common (and physiologically important) coupled reaction is protonation, as represented in the square scheme in fig. 2.  $K_{\text{Ox}}$  and  $K_{\text{Red}}$  are the acidity constants for Ox and Red. Utilising the principle of thermodynamic cycles (the sum of  $\Delta_r G^0$  values round the square is zero), these acidity constants can be linked to the reduction potentials of the protonated and un-protonated redox couples. Note that potentials alone cannot be summed; they must be scaled by  $n$ .

For an  $n$ -electron, one-proton process, the whole pH-dependence of the reduction potential is given by:

$$E^{0'}([H^+]) = E_{\text{alk}}^0 + \frac{2.3RT}{nF} \log_{10} \left( \frac{1 + \frac{[H^+]}{K_{\text{Red}}}}{1 + \frac{[H^+]}{K_{\text{Ox}}}} \right) \quad (9)$$

This equation is demonstrated in the appendix. Usually Red is a better base than Ox, so it has a higher  $pK_a$ , *i.e.*  $pK_{\text{Ox}} < pK_{\text{Red}}$ .

For  $pH < pK_{\text{Ox}}$ , both Ox and Red are protonated.



The reduction potential is  $pH$  independent, and equals  $E_{\text{acid}}^0$  (fig. 2).

For  $pH$  between  $pK_{\text{Ox}}$  and  $pK_{\text{Red}}$ , Ox is not protonated but Red is.



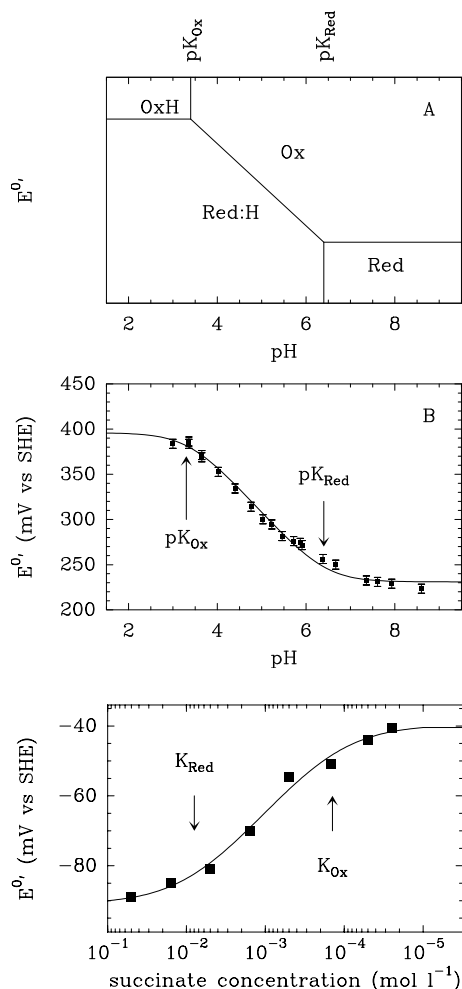


Figure 3: (A) Schematic Pourbaix diagram for the  $1e^-:1H^+$  reaction of amicyanin, a type I blue copper protein. (B) Reduction potential vs. pH for amicyanin from *Paracoccus versatus* at  $2^\circ\text{C}$ . The line is a best fit to eq. 9. The values of  $pK_{\text{Red}}$  and  $pK_{\text{Ox}}$  can easily be measured from the fit to eq. (9), with  $n = 1$ . Adapted with permission from ref. [23]. Copyright (2001) American Chemical Society.

Figure 4: Pourbaix-like diagram for the change in the reduction potential of the flavin cofactor of *E. coli* fumarate reductase as a function of succinate concentration (increasing from right to left) at  $20^\circ\text{C}$ , pH 7. Line is best fit to eq. (9), with  $n = 2$ , but with [succinate] instead of  $[H^+]$ . From ref. [24].

The reduction potential is pH dependent: it decreases by  $2.3RT/nF$  Volts per pH unit ( $-\frac{59}{n}\text{mV/pH}$  at  $25^\circ\text{C}$ ). This is simply understood as follows: the reduction potential increases as the concentration of protons increases because protonation makes reduction *easier* by consuming the reduced species.

For  $pH > pK_{\text{Red}}$ , neither Ox nor Red are protonated, the redox process is



The reduction potential is pH independent, and equals  $E_{\text{alk}}^0$  (fig. 2).

Redox-linked protonations are conveniently represented by a Pourbaix diagram, a plot of  $E^{0'}$  as a function of pH, as schematised in fig. 3A.

In general, for a redox process involving  $n$  electrons and  $m$  protons, the maximal pH-dependence is

$$-\frac{2.3RT}{F} \frac{m}{n} \text{V/pH unit} \quad (13)$$

As an example, fig. 3B [23] shows the dependence on pH of the reduction potential of the type-I copper site of amicyanin, determined using protein film voltammetry (see below, e.g. fig 10). The data can be analysed in terms of electron transfer being coupled to the protonation of a single

| Mediator  | $E^{0'}$ (mV vs SHE) |
|---|----------------------|
| Benzyl viologen                                     | -360                 |
| Lapachol  | -172                 |
| Methylene blue                                      | 11                   |
| Ferricyanide ( $\text{K}_3\text{Fe}(\text{CN})_6$ ) | 360                  |
| Hexachloroiridate ( $\text{Na}_2\text{IrCl}_6$ )    | 870                  |

Table 1: Standard reduction potentials at pH 7, 25°C, of common mediators.

group with  $pK_{\text{Red}} = 6.3$  and  $pK_{\text{Ox}} \leq 3.2$ . Protonation occurs on one of the two histidine ligands of the copper ion.

It is essential to understand that these considerations apply for any ligand which binds a redox center: provided that the dissociation constants from the reduced and oxidised forms are different, the reduction potential depends on the concentration of ligand, and the dissociation constants can be measured by determining how the reduction potential depends on the concentration of ligand. The latter may be the proton, the substrate/product or inhibitor of an enzyme, or even the apo-protein.

Figure 4 illustrates the succinate-concentration-dependence of the reduction potential of the active site flavin in *E. coli* fumarate reductase, determined using experiments such as those in fig. 22A. In this case, the reduction potential decreases as the concentration of succinate is raised (from right to left in this figure) because binding of succinate to the oxidised form of the enzyme is tighter than to the reduced form ( $pK_{\text{Ox}} > pK_{\text{Red}}$ ).

References [25–28] provide examples of the effect of protonation or binding of metal or exogenous thiolate on the reduction potential of FeS clusters.

## 2.5 Electron transfer (ET) kinetics

Electrons are transferred between the redox centers of redox proteins and enzymes involved in respiration and photosynthesis, and along chains of redox centers within certain enzymes. We first define the parameters that determine the *rates* of these homogeneous electron transfer (ET) events before discussing interfacial ET.

Let us consider a certain ET step, from a donor D to an acceptor A.



Thermodynamics predicts the ratio  $k_{\text{D} \rightarrow \text{A}}/k_{\text{A} \rightarrow \text{D}}$  (eq. 6) but not the values of the two rate constants. The rate of electron transfer (ET) from D to A depends on the reduction potentials of D and A (eq. 7), but also on other parameters. This was established in the 1960’s by Rudolph Marcus who developed a model based on a molecular description of ET between small molecules in solution and received the 1992 Nobel Prize in Chemistry for his theory. He showed that this process requires the formation of a transient complex, in which the kinetics of the ET step can be

described by an equation of the form

$$k_{\text{D} \rightarrow \text{A}} = C \exp \left( -\frac{(\Delta_r G^0 + \lambda)^2}{4\lambda RT} \right) \quad (15)$$

- $\Delta_r G^0$  is the standard free energy of the reaction, which is related to the standard reduction potentials of the donor D and the acceptor A according to  $\Delta_r G^0 = F(E_D^0 - E_A^0)$  (cf eq. 8).
- The parameter  $\lambda$ , called “reorganization energy,” is all the greater that large molecular rearrangements accompany the transfer (both the geometries of the molecules that are oxidized or reduced and the polarization of the surrounding solvent are considered). Biological electron transfers usually take place in the “normal region” ( $|\Delta_r G^0| < \lambda$ ), where the rate constant is increased when  $\Delta E^0$  increases and  $\lambda$  decreases, but the “inverted region” plays a very important role in photosynthetic electron transfers.
- The expression of the preexponential factor  $C$  depends on the strength of the electronic coupling between the acceptor and the donor. If it is strong enough (“adiabatic” transfer),  $C$  simply equates  $kT/h$ , as given by the classical transition state theory. When it is weak (this is so for long-distance, “nonadiabatic” ET),  $C$  depends on the overlap of the molecular wave functions of D and A, and therefore on the nature of the redox centers, on their distance and on the intervening medium. An exponential decrease of  $C$  with distance is observed [29]. In the literature, nonadiabatic transfers are often referred to as electron tunneling processes.

*The relation between thermodynamics and kinetics* is understood by calculating an equilibrium constant from the ratio  $k_{\text{D} \rightarrow \text{A}}/k_{\text{A} \rightarrow \text{D}}$  (then compare with eq. 3):

$$\frac{k_{\text{D} \rightarrow \text{A}}}{k_{\text{A} \rightarrow \text{D}}} = \frac{C \exp \left( -\frac{(\Delta_r G^0 + \lambda)^2}{4\lambda RT} \right)}{C \exp \left( -\frac{(-\Delta_r G^0 + \lambda)^2}{4\lambda RT} \right)} = \exp^{-\Delta_r G^0 / RT} \quad (16)$$

Now consider the electron transfer between a molecule and a **metallic electrode** (the case of semiconducting electrodes is treated e.g. in ref [1]).



The equation that gives the rate of ET is a complex function of the reduction potential of the molecule  $E^{0'}$ , the electrode potential  $E$ , and the reorganization energy  $\lambda$  [5, 18] but a simplified rate equation, known as the “Butler Volmer equation,” predicts that the rates of oxidation and reduction are independent on  $\lambda$  and exponentially increase and decrease (respectively) as the electrode potential increases:

$$k_{\text{ox}} = k_0 \exp \frac{F}{2RT} (E - E^{0'}) \quad (18a)$$

$$k_{\text{red}} = k_0 \exp -\frac{F}{2RT} (E - E^{0'}) \quad (18b)$$

The preexponential factor  $k_0$  depends on the coupling between the electrode and the redox

molecule. The greater  $k_0$  the faster the electron exchange between the electrode and the redox molecule; of course, this parameter has no physiological relevance.  $k_0$  is often called *the* rate of electron transfer, but it is important to understand that rates of ET depend on electrode potential, and the rate of ET equates  $k_0$  only when there is no driving force, at  $E = E^0$  (in which case  $k_{\text{ox}} = k_{\text{red}} = k_0$ ).

The relation between thermodynamics and kinetics is understood by calculating the ratio  $k_{\text{ox}}/k_{\text{red}}$  (then compare with eq. 5):

$$\frac{k_{\text{ox}}}{k_{\text{red}}} = \frac{k_0 \exp \frac{F}{2RT} (E - E^{0'})}{k_0 \exp -\frac{F}{2RT} (E - E^{0'})} = \exp \frac{F}{RT} (E - E^{0'}) \quad (19)$$

The more sophisticated Marcus-Hush model of interfacial ET takes into account the distribution of energy states in the metal; it gives eq. 18 justification when the overpotential is small (at  $E \approx E^0$ ), but in contrast, it predicts that the rate asymptotically approaches a plateau value  $k_{\text{max}}$  when the overpotential is greater than  $\lambda$ . An inverted region does not occur for an electrode reaction at a metal electrode. For further elaboration, see sections 1.4.2. in ref [5], or 3.6.2 in ref [3].

Since according to the Marcus-Hush model, the rate of interfacial electron transfer depends on  $E$  and  $\lambda$ , the dependence of the ET rate on  $E$  could be used to determine  $\lambda$ , which is a biologically relevant parameter. However, a complication arises from the fact that interfacial ET may be limited (“gated”) by a process that is distinct from ET. In that case, the plateau of the apparent ET rate may be incorrectly interpreted as the ET rate reaching the maximal value predicted by Marcus-Hush theory, and the reorganization energy may be greatly underestimated (for a discussion, see ref [30] and refs. therein).

## 2.6 Kinetics of proton-coupled electron transfer: stepwise versus concerted mechanisms.

When a redox process is coupled to proton transfer (judging from the pH dependence of the corresponding reduction potential), one can discern between *stepwise* mechanism (whereby electron transfer either precedes or follows proton transfer), and *concerted* mechanism (whereby both transfers occur simultaneously). The mechanisms can sometimes be discriminated on the basis of kinetic isotope effects, or from the dependence of rates on T, buffer, pH and/or  $\Delta G$  (or  $E$ ). Electrochemical investigations can be highly informative in this respect [31, 32]. We will discuss in section 6.2 simple electrochemical experiments that establish the stepwise mechanism of proton/electron transfer to a buried FeS cluster. Various examples of biologically-relevant coupled proton-electron transfers are discussed in [31].

## 3 Electrochemistry under equilibrium conditions: potentiometric titrations

The reduction potential of a redox couple is determined by recording the ratio  $[\text{Ox}]/[\text{Red}]$  observed after allowing the system to equilibrate with the electrode at different potentials.

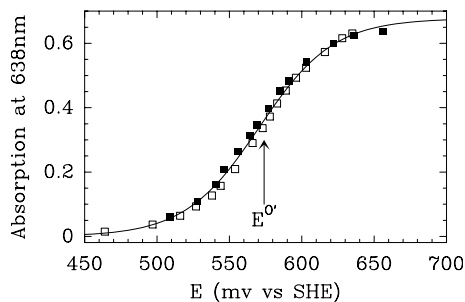


Figure 5: Potentiometric titration of *Pseudomonas aeruginosa* His117Gly azurin, a type-I blue copper protein (0.1mM protein, 20mM MES, pH 6, 33mM Na<sub>2</sub>SO<sub>4</sub>, 1M NaCl, 20°C.) The different symbols correspond to step-wise reduction and step-wise reoxidation. Plain line is best fit to eq. 20b with  $n = 1$ . The adsorption at 638nm is characteristic of the oxidised (blue) form of the copper center. Mediators: K<sub>3</sub>Fe(CN)<sub>6</sub>, Na<sub>2</sub>IrCl<sub>6</sub>, 1,2-ferrocene dicarboxyl acid. Adapted with permission from ref. [34]. Copyright (2000) American Chemical Society.

The potential is usually varied by adding titrants of an oxidant or a reductant. Unlike small molecules, protein redox centers do not generally react rapidly with the measuring electrode and equilibrium is not established quickly. To overcome this problem, small redox agents called mediators are added to the solution to transport electrons between the active site and the electrode. For best results, these should have reduction potentials close to that of the active site being studied; mixtures of mediators are often employed to cover a wide range. A short list of mediators and their reduction potentials is given in table 1. See also ref [33].

The ratios [Ox]/[Red] are typically determined by examination of the optical or EPR spectra. Very often, the concentration of Ox or Red is measured as a function of the electrode potential, and the data are fitted with:

$$[\text{Red}] \propto \frac{1}{1 + \exp\left(\frac{nF}{RT}(E - E^{0'})\right)} \quad (20a)$$

$$[\text{Ox}] \propto \frac{\exp\left(\frac{nF}{RT}(E - E^{0'})\right)}{1 + \exp\left(\frac{nF}{RT}(E - E^{0'})\right)} \quad (20b)$$

Fig. 5 is the result of a potentiometric titration of the “blue” (type-I) copper site in an azurin mutant, followed by UV-vis spectroscopy. The oxidized copper site absorbs at  $\approx 600\text{nm}$  due to a Cys-S to Cu ligand-to-metal-charge-transfer, and the intensity of this band is therefore proportional to the concentration of oxidized copper site.

Performing such experiment under fully anaerobic conditions requires a glove-box... or skills. Dutton described the glassware that can be used on the bench for the anaerobic potentiometric preparation of samples to be examined by EPR or UV-Vis spectroscopy [35, 36].

## 4 Dynamic electrochemistry

### 4.1 Distinction between equilibrium and dynamic electrochemistry

In potentiometry experiments (sec. 3), the measurement of the electrode potential is carried out under equilibrium conditions: the stepwise addition of titrant makes the concentrations change, but when equilibrium is reached the rates of oxidation and reduction exactly cancel each other and there is no net transformation. The reduction or oxidation is detected by spectroscopy, and therefore this approach requires that the redox center has a distinct spectroscopic signature.

A completely different approach consists in forcing the electrode potential to take a value that is different from the equilibrium potential. In that case, the system may evolve towards equilibrium by taking electrons from (of giving electrons to) the electrode. This reduction (resp. oxidation) is detected as a current (in unit of Ampere, that is Coulomb/second) which measures the amount of electric charge passing the electrode per unit time. Therefore it is proportional to the *rate* of reduction or oxidation.

## 4.2 Electrodes for electron transfer to/from proteins

To be successful, electrodes must exchange electrons quickly with the proteins, and preserve their native properties. These electrodes may resemble natural environments or reaction partners for the protein.

Electron transfer can be achieved if the redox center is exposed at the protein surface (or not too deeply buried). In the case of enzymes whose active site is buried in the protein, a favorable situation occurs when it is “wired” to the surface by a chain of redox cofactors; having one of these centers exchanging electrons with the electrode is enough for achieving an electric connection of the active site. Direct ET to enzymes was first reported in the late 1970’s [37, 38] and is now very common, but not all redox enzymes can be electrically connected to electrodes.

Protein/electrode interactions may be tailored to be weak or strong. Weak interactions might ideally give rise to diffusion-controlled electrochemistry (section 5), whereas with strong interactions, the experiment may address just a small sample (“film”) of protein molecules on the electrode (sections 6 and 7).

Electrode surfaces for which protein electrochemistry is commonly observed are listed below:

- Metal (Au, Pt, Ag) surfaces on which a monolayer of adsorbate is self assembled (“Self Assembled Monolayers” or SAMs [39]). The adsorbate is a bi-functional molecule of the type  $X-(CH_2)_n-Y$ , where X is a substituant that anchors the molecule on the metal electrode surface (e.g. a thiol) and Y is a functional group that interacts with the protein (typically carboxyl for cytochromes *c*, or amino for acidic proteins such as plastocyanin or ferredoxins.)
- Pyrolytic graphite edge [40] or basal plane electrodes provide hydrophylic or hydrophobic interactions, respectively. The former is sometimes used with co-adsorbates (aminocyclitols, polymyxin, polylysine) which probably form cross-linkages between the protein and the electrode surface.
- Graphite or carbon nanotubes can be functionalized by reducing a diazonium salt [41] to expose aromatic functionalities [42] or amino groups [43, 44] that interact favorably with hydrophobic or carboxylate-rich patches on the protein surface. Carbodiimide coupling can then be used to form an amide bond between amino groups on the electrode surface and protein carboxylates (or *vice versa*).
- Various electrode materials covered with either a film of non-biological surfactant (e.g. DDAB) or layers of polyions have been used to incorporate large membrane-bound proteins, but catalytic activity was generally greatly impaired. Suitable electrodes for integral membrane enzymes are described in refs [19, 45].

When the protein that is studied is an enzyme, proof that it is not denatured on the electrode is that it can still catalyse the transformation of its physiological substrate *at a reasonable rate and in a range of electrode potential that is consistent with what we know about the catalytic cycle and the redox properties of the cofactors*. Checking the effects of known specific inhibitors can also be useful. Upon starting a new project, and before embarking on detailed electrochemical studies, it is essential to make sure that the catalytic properties of the adsorbed enzyme bear some resemblance to those determined in biochemical experiments. In this chapter, we illustrate this by also discussing the results of conventional experiments which confirm certain unexpected results obtained in electrochemical investigations of redox enzymes.

### 4.3 Electrochemical equipment

The experiment is carried out using an electrochemical analyser in conjunction with the cell. The cell consists of three electrodes. The reference electrode is often contained in a side arm linked to the main compartment by a capillary tip called a Luggin (after the glassblower who invented it). The tip is positioned close to the working electrode. To avoid passing current through the reference electrode (this would change its potential and also damage it), a third electrode, called auxiliary or counter electrode, is used. The working electrode can also be rotated (sections 5.2 and 7) to control mass transport of solution species.

The analyser measures the current registered in response to the potential that is applied. In general, the potential of the working electrode (versus the reference electrode) is modulated (e.g. in a linear sweep) and the current flowing between the working electrode and the counter electrode is recorded. Since the electrode potential is swept forward and back, the technique is called “cyclic voltammetry”. The scan rate  $\nu$  (in units of V/s) is a very important parameter which determines the time-scale of the experiment and therefore the time constant of the processes which can be resolved [5]. A voltammogram is a plot of current against electrode potential. Alternatively, in an experiment called “chronoamperometry”, the electrode potential is held at a fixed value (or sometimes stepwise changed) and the current is recorded as a function of time.

### 4.4 Vocab and conventions

A cathodic process is a reduction, the cathode is the electrode onto which the reduction occurs. An anodic process is an oxidation, occurring at the anode.

In Europe, a cathodic current is counted as negative and an oxidation results in a positive current. American people and softwares often use the opposite convention for the sign of the current (see e.g. fig. 7).

### 4.5 The capacitive current

The measured current is usually the sum of a Faradaic current (which reveals the redox transformations of molecules that come sufficiently close to the electrode) and a capacitive current  $i_c$ , which does not involve the passage of electrons across the electrode-solution interface. The capacitive current (or “charging current”) arises as a consequence of the variation of the electrode

potential and it is proportional to the electrode surface  $A$ :

$$i_c = C \frac{dE}{dt} = C\nu \quad (21)$$

where  $C$ , the capacitance of the electrode/electrolyte interface, is proportional to  $A$ .

In a voltammetric experiment, the magnitude of the capacitive current is therefore proportional to scan rate  $\nu$ . It is positive if  $E$  is increasing and negative if the electrode potential is swept down.

There is no capacitive contribution to the current if the potential is constant, but potential steps (in chronoamperometry experiments) result in current transients that are approximately exponential ( $i_c < 0$  if the potential is stepped down,  $i_c > 0$  if the potential is stepped up). This current usually decays in less than a few seconds.

The capacitive current must be subtracted from the total current to obtain the Faradaic contribution. It can sometimes be determined from a control experiment where there is no Faradaic current, or extrapolated from the part of the signal where there is no Faradaic contribution (see e.g. fig 10) [46].

## 5 Diffusion controlled Voltammetry

### 5.1 Diffusion controlled voltammetry at stationary electrodes

We consider a solution containing only the reduced form of a soluble electroactive species, and the potential is swept linearly in time, as shown in fig. 6A, starting from a low potential. The current response as a function of time is plotted in fig. 6B, and the cyclic voltammogram (current against potential) in fig. 6C.

While the potential is lower than  $E^{0'}$ , no oxidation occurs and no current is measured [see (a) in figs. 6]. This is because the rate of oxidation  $k_{\text{ox}} = k_0 \exp\frac{F}{2RT}(E-E^{0'})$  is much lower than the rate of reduction  $k_{\text{red}} = k_0 \exp\frac{-F}{2RT}(E-E^{0'})$  (section 2.5). When the electrode potential approaches  $E^{0'}$ , Red starts being oxidised into Ox, giving electrons to the electrode. This is measured as a (positive) current which increases as  $E$  and the rate of oxidation increase (b). However, the electrode oxidises only species adjacent to it and the interface is soon depleted. The current reaches a maximum before it starts to decrease (c). It tends to zero like  $t^{-1/2}$  (noting that  $E$  changes in proportion to time  $t$ ). This decrease in current reveals that the size of the diffusion layer (i.e. the zone of the solution adjacent to the electrode where the concentration of species differ from that in the bulk) increases by diffusion like the square root of time, and the concentration gradient that drives the diffusion of Red from the bulk of the solution to the interface therefore decreases like  $t^{-1/2}$ .

While a positive current is being measured, Ox produced by the reaction accumulates near the electrode and diffuses slowly towards the bulk.

After the scan is reversed, (d), the current is still positive and decreasing: Red species are still being oxidised since the electrode potential is above the reduction potential. Near the reduction potential, the Ox species which have accumulated are now being reduced and a negative current is observed (e) until the concentration of Ox near the interface drops down (f), and so does the magnitude of the current.

This results in a peak-like response in both directions. The modeling of voltammograms is

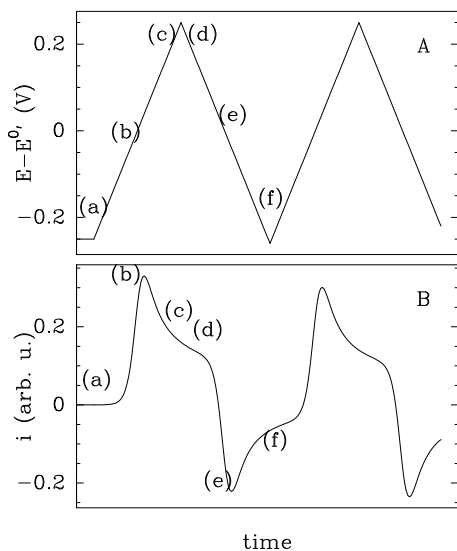


Figure 6: Cyclic voltammetry for a **redox species free to diffuse in solution**, at a **stationary electrode**. In a typical voltammetric experiment, the electrode potential is swept linearly in time (A), and the current recorded as a function of time (B). A convenient and usual way of displaying the results is to plot the current against potential (C). The labels (a) to (f) are referred to in the text. “arb. u.” means “arbitrary units”.

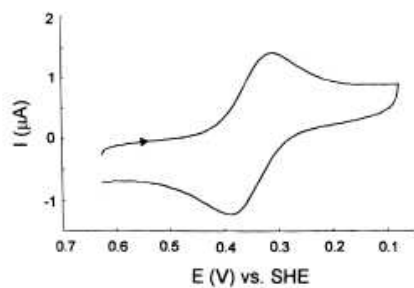
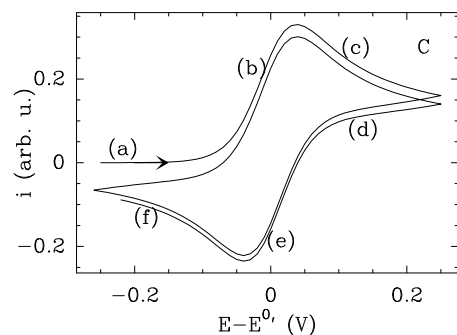


Figure 7: Data for diffusion limited voltammetry of a redox protein, the cytochrome  $c_2$  from Rps. palustris.  $C = 0.2\text{mM}$ , cell volume  $0.5\text{mL}$ . From ref. [47]. Mind the axis! The voltammogram is plotted with the American convention: the high electrode potentials are on the left, and the current is positive for a reduction. Reprinted with permission from ref. [47]. Copyright (1997) American Chemical Society.

complex (chapter 6 in [1]) because the current response depends on the free diffusion of the species in solution, and the differential equations coupling reaction and diffusion are in general difficult to solve.

For an  $n$ -electron reaction, the separation between cathodic (reduction) and anodic (oxidation) peaks is given by

$$\Delta E_p = E_{p,a} - E_{p,c} = 2.218 \frac{RT}{nF} = \frac{57}{n} \text{mV at } 298\text{K} \quad (22)$$

The peak current is proportional to the bulk concentration of species  $C$ , and to the square root of the potential scan rate  $\nu$ :

$$i_p = 2.69 \cdot 10^5 n^{3/2} A D^{1/2} \times C \sqrt{\nu} \quad (23)$$

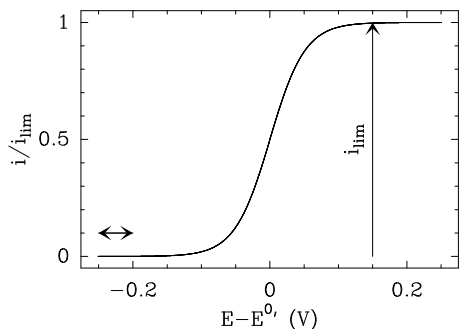


Figure 8: Sigmoidal wave obtained in a cyclic voltammetry of an **electroactive species in solution** at a rotating disc electrode.

This is the Randles-Sevcik equation.  $A$  is the electrode surface,  $D$  is a diffusion coefficient. A linear plot of  $i_p$  against  $\sqrt{\nu}$  is the criterion used to identify when the redox species are diffusing from the bulk to the electrode.

A system that conforms to these criteria is said to be *reversible* and *diffusion controlled*, and the reduction potential is obtained from the average of the cathodic and anodic peak potentials.

$$E^{0'} \approx \frac{E_{p,a} + E_{p,c}}{2} \quad (24)$$

Figure 7 shows a voltammogram for the reversible oxidation and reduction of a cytochrome. Note that the concentration of the protein sample must be high. For example the experiment in fig. 7 used 100nmol of cytochrome.

Deviation from this ideal behavior might arise when interfacial electron transfer is slow (in which case the peaks broaden and tend to separate), or when one of the redox species is irreversibly transformed on the voltammetric time scale (in which case the signal might become asymmetrical) (see chapter 2 in ref [5] for the effect of follow-up reactions on the voltammetry of diffusive species, and section 6.2 herein for an example with an adsorbed protein).

## 5.2 Diffusion controlled voltammetry at rotating electrodes

The peak shape of the diffusion-limited voltammogram at a macro electrode is due to the depletion of electroactive species near the electrode surface as they are consumed by the redox reaction.

There are many electrochemical techniques in which the solution moves with respect to the electrode. In the most popular configuration, the electrode (called a “rotating disc electrode”) is rotated along its axis in the solution. This introduces a *convective* movement of the solution which increases the efficiency of the transport of species from the bulk towards the electrode. Because the depletion layer can no longer spread in the solution, the current reaches a limiting value  $i_{lim}$  at high driving force, fig. 8.

The Levich equation predicts that the limiting current is proportional to the concentration of electroactive species  $C$  and to the square root of the electrode rotation rate  $\omega$ :

$$i_{lim} = 0.620nFA\nu_s^{-1/6}D^{2/3} \times C\sqrt{\omega} \quad (25)$$

In this equation,  $\nu_s$  is the kinematic viscosity of the solution. (The kinematic viscosity is the ratio of the viscosity over the density. *E.g.* the viscosity of pure water at 20°C is 10<sup>3</sup>μPa·s, and its

density  $\approx 1\text{g/cm}^3$ ; this gives a kinematic viscosity  $\nu_s \approx 10^{-2}\text{cm}^2/\text{s}$ .) A plot of  $i_{\text{lim}}^{-1}$  against  $\omega^{-1/2}$  is called a Koutecky-Levich plot. The reduction potential  $E^{0'}$  is simply given by the half-wave potential  $E_{1/2}$ , the potential at which the current reaches half its limiting value.

$$\boxed{E^{0'} = E_{1/2}} \quad (26)$$

The scan rate  $\nu$  and direction do not enter the measurement if  $\nu$  is small. When the current depends on electrode potential but is independent of time, the voltammogram is said to be at *steady state*.

This configuration is not used for measuring the reduction potential of redox proteins, because rotating the electrode in the solution requires that the volume of the electrochemical cell be large, but it is important to understand the difference between this experiment and that show in fig 22A, since they give similar electrochemical responses for completely different reasons.

The above considerations only apply to “macro”-electrodes (*i.e.* when the diameter of the electrode is larger than the typical size of the diffusion layer). With a “micro”-electrode, whose typical size is of the order of a few micrometers, the voltammogram may have a sigmoidal shape even in the absence of convection (sec 5.2.2 in [1]). Reference [48] shows cyclic voltammograms of amicyanin from *P. denitrificans* at a  $3\mu\text{m}$  gold micro electrode. Micro-electrodes have also been used in the context of cell biology; their size make them suitable to detect electroactive species released by a single cell. See e.g. ref [49] for a recent review.

## 6 Voltammetry of adsorbed proteins: Protein Film Voltammetry (PFV)

When the protein is immobilised on the electrode surface, diffusion is eliminated and much greater thermodynamic and kinetic resolution can be obtained with extremely small sample quantities. This approach was developed by F. Armstrong (now in Oxford) in the 1970’s with small redox proteins, and since the beginning of the 1980’s with large redox enzymes. Over the last years, this technique was used to study all sorts of aspects of the mechanism of redox proteins and enzymes [18]: proton transfer [50] (cf section 6.2), inter and intramolecular electron transfer [51,52], diffusion along substrate channels [53,54] (section 5) etc. The rest of this article will focus on the principle and applications of protein film voltammetry.

### 6.1 Non-catalytic voltammetry at slow scan rates to measure reduction potentials

Figure 9 shows the ideal shape of a cyclic voltammogram when the redox species is adsorbed onto an electrode [1].

Starting again at an electrode potential lower than  $E^0$ , the redox centers are fully reduced [see (a) in fig. 9]. Sweeping the potential towards high values, the protein starts being oxidised when the electrode potential approaches the reduction potential (b); a positive current is then measured, which drops down to zero at high potential when all the adsorbed protein molecules have been oxidised (c). On the reverse scan, a reductive (negative) current is observed when the

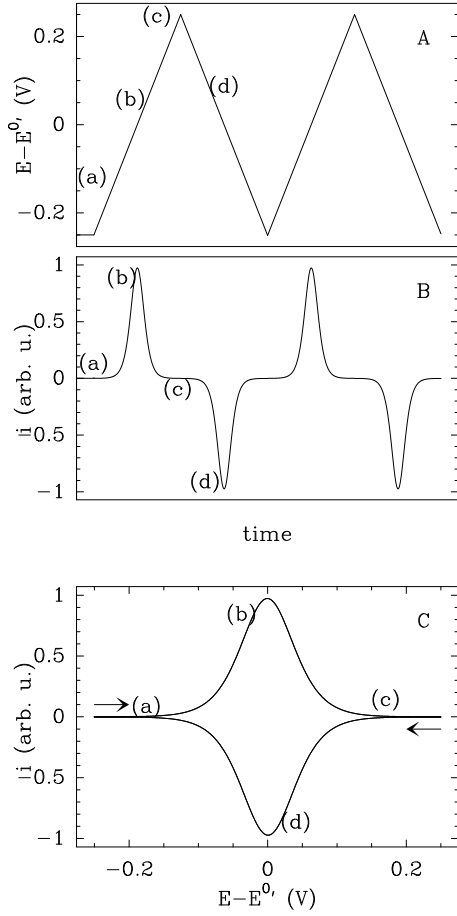


Figure 9: Cyclic voltammetry for a **redox species adsorbed on an electrode surface**. Rotation of the electrode should make no difference. In a typical voltammetric experiment, the electrode potential is swept linearly in time (A), and the current recorded as a function of time (B). Panel C shows the cyclic voltammogram.

electrode potential matches the reduction potential of the protein (d) until the entire sample has been reduced and the current vanishes.

For an ideal, reversible system, the signal consists of symmetrical oxidation and reduction peaks centered at the reduction potential  $E^0'$ .

$$\boxed{E^0' = E_{p,c} = E_{p,a}} \quad (27)$$

The area under the peak ( $\mathcal{A}$ , in units of VA) gives the charged passed for that redox couple ( $nF$  electrons per mole of adsorbed centers,  $\Gamma A$ ,  $A$  is the electrode surface). It should be the same for the oxidative and for the reductive peaks.

$$\mathcal{A} = nFA\Gamma\nu \quad (28)$$

The peak current is proportional to the scan rate  $\nu$ , to the surface concentration of electroactive species  $\Gamma$  and to the square of  $n$ . Therefore, the electroactive coverage must be high enough for a current to be observed. Typically, a coverage higher than  $5\text{pmol}/\text{cm}^2$  will suffice.

$$i_p = \frac{n^2 F^2 A \Gamma \nu}{4RT} \quad (29)$$

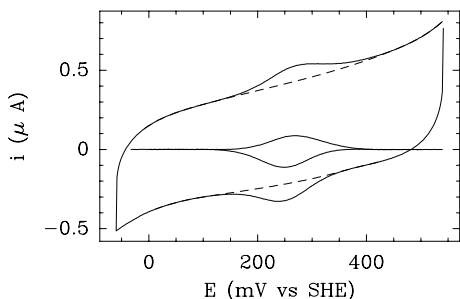


Figure 10: Cyclic voltammogram for *Pseudomonas aeruginosa* azurin adsorbed at a pyrolytic graphite electrode. The dashed line is the baseline and the inset shows the baseline subtracted current (the Faradaic current).  $0^\circ\text{C}$ , pH 8.5.  $\nu = 20\text{mV/s}$ .  $\Gamma_A \approx 5.5\text{pmol}$ .

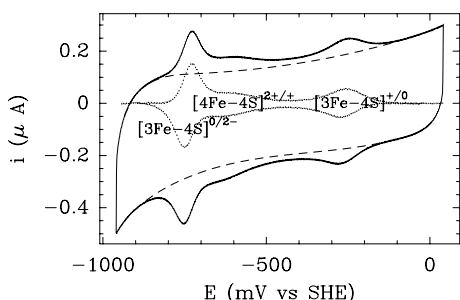


Figure 11: Cyclic voltammogram for *Sulfolobus acidocaldarius* 7Fe ferredoxin adsorbed at a pyrolytic graphite electrode [55]. The dashed line is the baseline.  $0^\circ\text{C}$ , pH 8.5,  $\nu = 20\text{mV/s}$ .  $\Gamma_A \approx 3.5\text{pmol}$ .

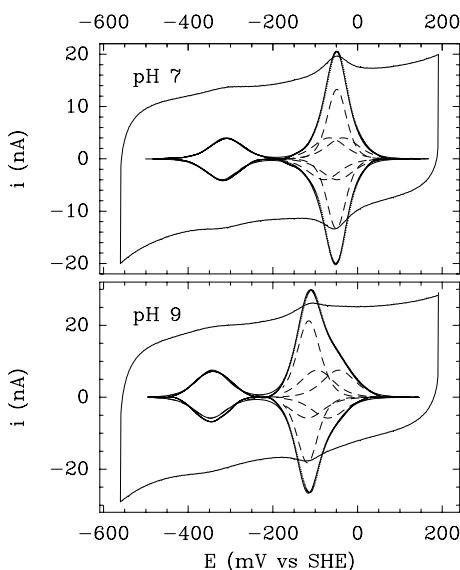


Figure 12: Cyclic voltammograms (raw data out of scale, base-line subtracted and deconvoluted signals) for *E. coli* fumarate reductase (FrdAB) adsorbed at a pyrolytic graphite edge electrode. This enzyme contains 3 FeS clusters and a flavin cofactor.  $20^\circ\text{C}$ , pH 7 (top panel) & 9 (bottom panel),  $\nu = 10\text{mV/s}$ . At pH 7, FADox/FADred  $-50\text{mV}$  vs SHE,  $[2\text{Fe}2\text{S}]^{2+/+} -40\text{mV}$ ,  $[4\text{Fe}4\text{S}]^{2+/+} -305\text{mV}$ ,  $[3\text{Fe}4\text{S}]^{+/0} -65\text{mV}$ .  $\Gamma_A \approx 0.4\text{pmol}$ . Note the strong pH dependence of the FAD signal. Adapted with permission from ref [24]. Copyright (2001) American Chemical Society.

A linear plot of  $i_p$  against  $\nu$  proves that the redox species are adsorbed onto the electrode.

The peak width at half height,  $\delta$ , is:

$$\delta \approx 3.53 \frac{RT}{nF} \quad (30)$$

( $\frac{91}{n}$  mV at  $25^\circ\text{C}$ ). Note that the expected dependence on temperature is not observed in experiments [55, 56].

Cooperative two-electron transfers give signals with up to four times the height and half the width of one electron transfers; they are therefore more easily distinguished.

Figure 10 shows a non-catalytic voltammogram that makes it possible to determine the redox potential of the copper site of azurin. In experiments, there is a capacitive contribution resulting

from “electrode charging” (section 4.5). The dashed line shows the interpolated capacitive current which has to be subtracted to obtain the Faradaic current alone.

Figure 11 shows the voltammetry of the 7Fe ferredoxin of *Sulfolobus acidocaldarius*, which contains one [3Fe4S] cluster, with redox transitions  $[3\text{Fe4S}]^{+/0}$  and  $[3\text{Fe4S}]^{0/2-}$ , and one [4Fe4S] cluster with a 2+/+ redox transition. When different centers are present in a protein, the different redox transitions appear as multiple peaks, the areas of which reveal the stoichiometry of the redox processes. *E.g.* the area under the low potential  $[3\text{Fe4S}]^{0/2-}$  peak is twice as much as that of the high potential  $[3\text{Fe4S}]^{+/0}$  peak. This figure also illustrates the fact that 2-electron redox processes give prominent signals (cf. eqs. 29 and 30).

The fumarate reductase from *E. coli* contains 3 FeS clusters and one flavin cofactor. The 2-electron signal associated with the flavin is easily distinguished from the three one-electron peaks due to the FeS clusters (fig. 12). The data clearly show that the reduction potential of the FAD is strongly pH dependent, as expected for a reduction process coupled to protonation (cf. sec 2.4). The fact that the peak shifts about  $-60\text{mV}$  between pH 7 and 9 shows that this corresponds to a 2-electron one-proton reaction (cf eq. 13).

Voltammetry is now becoming a routine technique to measure reduction potentials, and offers several advantages over potentiometric titrations described in sec. 3:

- *No need for a spectroscopic “handle”.* There is no requirement for a distinctive and unambiguous change in some spectroscopic parameter. The counterpart of this advantage is obvious: voltammetry provides no structural information.
- *Sample economy.* A few pmol of protein/enzyme are adsorbed onto the electrode (although making a film sometimes requires a larger amount than that, typically ten to one hundred times as much, this is still much less than required for bulk titration)
- *Quick measurements.* Recording a cyclic voltammogram usually takes a few seconds to a few minutes.
- *Instantaneous dialysis.* The electrode can be transferred in a solution of different composition/pH and the measurement repeated with the same sample. The protein might even survive long enough in a hostile environment for measurements to be performed before the electrode is taken back into a more gentle solution (see e.g. ref. [25] for the measurement of the reduction potential of a [2Fe2S] cluster in the pH range from 2 to 14).
- *Easier analysis & modeling of data.* The baseline (the charging current) is easily removed, and interpretation of non-catalytic data does not require solving any transport (diffusion/convection) equation.
- *In situ measurements.* Reduction potentials can be measured as a function of temperature [55,57–59] or even pressure [60].

## 6.2 Fast scan voltammetry to determine the rates of coupled reactions

The measurement of a reduction potential (an equilibrium property) theoretically requires that the system is at equilibrium. This appears to be in contradiction to measuring a current: indeed,

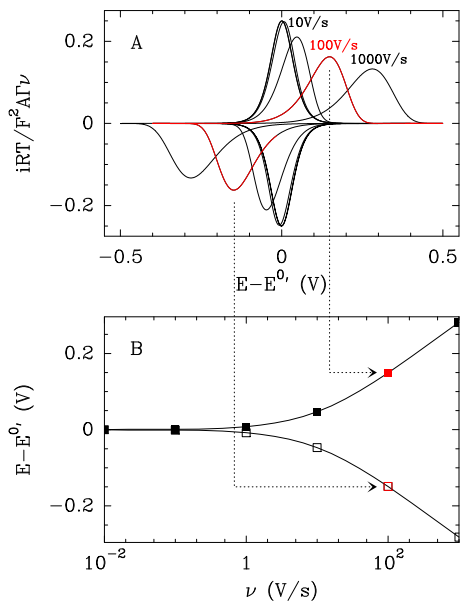


Figure 13: Effect of scan rate on the voltammetry of a redox species undergoing a one-electron, no-proton redox process, with  $k_0 = 0.1\text{s}^{-1}$ . A: calculated cyclic voltammograms at different scan rates (from 1000V/s to 10mV/s). The difference between  $E_{p,a}$  and  $E_{p,c}$  increases as the scan rate is raised. B: “Trumpet plot”:  $E_{p,a}$  (filled squares) and  $E_{p,c}$  (empty squares) as a function of the log of the scan rate. The slower electron transfer rate is, the peak will separate at a slow scan rate and the trumpet plot will shift to low scan rates.

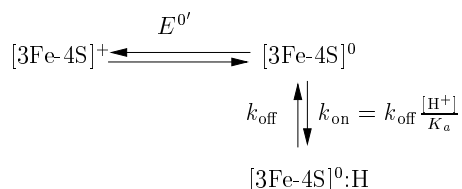


Figure 14: L-shape scheme used to interpret the fast scan voltammetry of a [3Fe4S] cluster. Electrochemists call this an “EC” mechanism [2, 5].

the flow of electrons when the protein is oxidised or reduced results from the fact that the system is driven out of equilibrium when the electrode potential is changed around the (equilibrium) reduction potential. In practice, this does not matter too much if the scan rate (and therefore the current) is slow enough that the system is *nearly* at equilibrium [61]. When the scan rate is raised, however, departure from equilibrium can be observed, and a great deal of information about the *kinetics* of redox processes can be gained by looking at the scan rate dependence of the voltammograms.

Theoretical voltammograms for an uncoupled one-electron redox process are plotted in fig. 13A. At slow scan rate, the oxidation peak occurs at  $E^{0'}$ . If the scan rate is high, because it takes time for the electron transfer between the electrode and the redox center to occur, the maximal current is observed *after* the redox potential has been reached, i.e. at higher electrode potential. The same reasoning applied to the reductive process predicts that  $E_{p,c}$  is lower than  $E^{0'}$ .

When measurements are performed over a large range of scan rates, the results can be displayed by plotting  $E_{p,a}$  and  $E_{p,c}$  as a function of scan rate, on a log scale, as shown in fig. 13B [61]. This has been called a trumpet plot. The more efficient the electron transfer between the electrode and the active site (the greater  $k_0$  in eq. 18), the higher the scan rate at which the oxidative and reductive peaks start to separate (peak separation occurs when the scan rate is greater than about  $k_0 RT/F$  [61]). For adsorbed redox proteins, reported values of  $k_0$  vary greatly, from a few inverse seconds to  $15000\text{s}^{-1}$ , in which case the peaks remain visible at scan rates as high as 3000 V/s [62, 63]. Needless to say, the situation of fast ET is more desirable if the focus is on studying biologically relevant processes rather than interfacial electrochemistry.

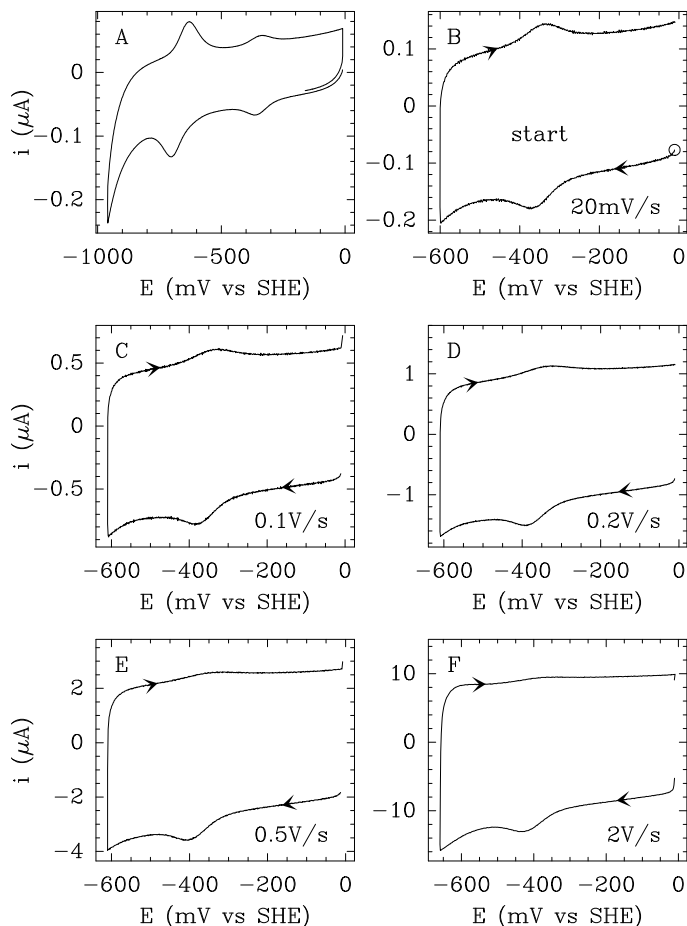


Figure 15: Effect of scan rate on the voltammetry of a redox species undergoing a one-electron, one-proton redox process. The data are for the  $[3\text{Fe}_4\text{S}]^{+/0}$  redox couple of a slow proton-transfer mutant of *Azodobacter vinelandii* ferredoxin I (D15E) at low pH [50, 64].

Fast scan voltammetry also gives information about the rates of the reactions that are coupled to ET. If these coupled reactions (e.g. (de)protonation) are fast on the voltammetric time scale, their effect is to shift the reduction potential of the redox couple (section 2.4), and also to decrease the apparent rate of electron transfer, the parameter noted  $k_0$  in eq 18 (this effect is discussed in a series of papers written by Etienne Laviron in the 1980's [65,66], see also [32] and section 2.1.2.1 in ref [18]). In that case, the voltammogram remains reversible at very low scan rate, and symmetrical but with greater peak separation when the scan rate is increased (fig. 13).

Recording voltammograms at increasing scan rates can be used for determining the value of  $k_0$ , but also to determine the rates of chemical processes that are coupled to electron transfer. From a biological point of view, proton transfer is certainly the most important reaction coupled to electron transfer, because the synthesis of ATP in most organism is coupled to long range proton transfers across biological membranes [67], but the kinetics and mechanism of proton transfer are difficult to study using conventional techniques. It is remarkable that electrochemistry proved very useful in this context [50,64], as described below.

Fig. 15 illustrates the voltammetric study of the  $[3\text{Fe}_4\text{S}]^{+/0}$  one-electron one-proton reaction (fig. 14), for a mutant of *Azodobacter vinelandii* ferredoxin I. High-resolution crystal structures reveal that the  $[3\text{Fe}_4\text{S}]$  is buried with no access to water molecules, and that a carboxylate group from an aspartate (D15) is located close to the cluster on the protein surface. It was suggested that a movement of this position 15 side chain may transfer a proton from the solvent to the cluster.

The experiments depicted in fig. 15 illustrate the use of fast-scan voltammetry to determine the kinetics of protonation of the [3Fe4S] cluster in a mutant where D15 is replaced with a glutamate. They were performed at pH 5.4, greater than  $pK_{\text{Ox}}$  and 1.3 pH unit lower than the  $pK_{\text{Red}} = 6.7$  of the [3Fe4S] cluster, the reduced form of which is therefore protonated at equilibrium. The scans were started from the high potential limit, and only the first scan is considered.

- At slow scan rates (panels A and B in fig. 15) oxidation and reduction peaks for the [3Fe4S]<sup>+0</sup> appear at the same electrode potential ( $\approx -350\text{mV}$ ). Under these “close-to-equilibrium” conditions, the reduction is followed by protonation, and oxidation proceeds along the reverse route (fig. 14).
- When the scan rate is increased, oxidation and reduction peaks start to separate (fig. 15C).
- At scan rates between 1 and 10V/s, the reductive peak is still clearly visible, but the oxidation peak vanishes (fig. 15D to F), because the cluster is trapped in the protonated form: it is quickly protonated upon reduction, but the rate of de-protonation,  $k_{\text{off}}$  in fig. 14, is too small for the cluster to be de-protonated during the fast oxidative scan. The deprotonation of the cluster “gates” its reoxidation.
- At very high scan rates, 20V/s and above (not shown), both peaks are observed, but the average reduction potential is lower than at low scan rate, and matches the alkaline limit: this is because the scan is reversed before the reduced cluster is protonated, and electron transfer is therefore not coupled to protonation.

These very simple experiments determine the rates of (de)protonation. Electrochemistry can achieve this because the time scale of potential modulation can be changed over orders of magnitude (1 min at 10mV/s to 1 ms at 1000V/s) to match that of the chemical events. In conjunction with site-directed mutagenesis, crystallography, and molecular dynamics simulations, this made it possible to obtain very original information about the molecular mechanism of protonation [50,64].

Several examples of voltammetric studies of coupled reactions, involving cytochromes and FeS clusters, have been reported (see e.g. [30,34,68]).

## 7 Catalytic protein film voltammetry and chronoamperometry

### 7.1 Principle and general comments

In the absence of substrate and at sufficiently high coverage, a redox enzyme immobilized onto an electrode gives peak-like signals resulting from the reversible transformation of its redox centers (fig. 12). Upon adding substrate, the non-turnover peaks are transformed to sizeable “catalytic waves” [69]: reaction with substrate transforms the active site, which is regenerated by electron exchange with the electrode in a succession of catalytic cycles. The magnitude of the current is proportional to electroactive coverage and to turnover rate, and so the relationship between driving force (potential) and catalytic activity is traced in a single voltammetric experiment. Note that catalysis may be observed even if coverage is too low to observe non-catalytic signals (as is unfortunately often the case).

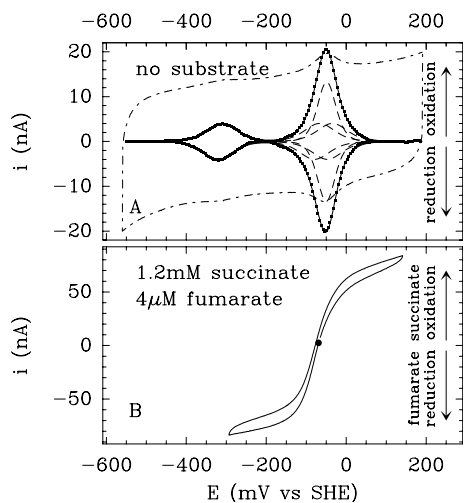


Figure 16: (A) Non-catalytic voltammogram obtained for *E. coli* fumarate reductase (FrdAB) adsorbed at a pyrolytic graphite edge electrode in the absence of substrate. The raw voltammogram (outer dash-dot line) is not to scale. Inset: background corrected current (small dots) and deconvoluted data (dashed lines).  $\nu = 10\text{mV/s}$ ,  $20^\circ\text{C}$ , pH 7. See also fig. 12. (B) Catalytic wave showing reversible succinate oxidation and fumarate reduction by adsorbed FrdAB in a solution containing succinate and fumarate, with the electrode rotating at a high rate.  $\nu = 1\text{mV/s}$ ,  $20^\circ\text{C}$ , pH 7,  $\omega = 3000\text{rpm}$ . Adapted with permission from ref [24]. Copyright (2001) American Chemical Society.

We shall discuss qualitatively a series of voltammograms and chronoamperograms obtained with 3 different enzymes and selected because they illustrate the variety of experiments that can be carried out and the variety of information that can be obtained. We shall emphasize what makes each result particularly relevant in the context of mechanistic studies. These three enzymes are

- The soluble fraction of *E. coli* fumarate reductase (FrdAB), a flavoenzyme that has a electron transfer chain consisting of three FeS clusters [70]. Its physiological function is to reduce fumarate to succinate, but it can also oxidize succinate both *in vitro* and *in vivo*, when it replaces succinate dehydrogenase (complex II).
- Various hydrogenases (from *A. vinosum*, *D. fructosovorans* and *A. aeolicus*) in which the NiFe active site is connected to the protein surface by a chain of three FeS clusters and a gas channel [53, 71]. These enzymes reversibly catalyse the oxidation of  $\text{H}_2$ .
- The periplasmic nitrate reductase from *R. sphaeroides* (NapAB), which irreversibly reduces nitrate into nitrite. This enzyme houses a buried molybdenum active site, one 4Fe4S cluster and two surface exposed hemes [72].

The non-catalytic voltammetry of *E. coli* fumarate reductase has been discussed above (fig. 12). Figure 16 shows again the non-catalytic voltammetry of this enzyme in panel A and the catalytic signal that is observed when the solution contains both fumarate and succinate and the electrode is rotated at a high rate to avoid mass-transport control (panel B). The flavin cofactor is oxidised at high electrode potential, giving 2 electrons to the electrode. The oxidised enzyme can bind succinate, and the oxidation of succinate results in the reduction of the flavin. The reduced FAD can be re-oxidised giving electrons to the electrode and so on. This results in a steady-state flux of electrons from succinate in solution to the electrode, *via* the adsorbed enzyme, which is measured as a steady-state positive current. At low electrode potential, a reductive (negative) current is observed which is proportional to the rate of fumarate reduction.

The filled circle in fig. 16B indicates the potential of zero net current (or “open circuit potential”, OCP) at  $-51\text{mV}$ . This corresponds to the reduction potential of the fumarate/succinate couple which can be calculated for any concentration ratio using the Nernst equation (eq. 5) and the

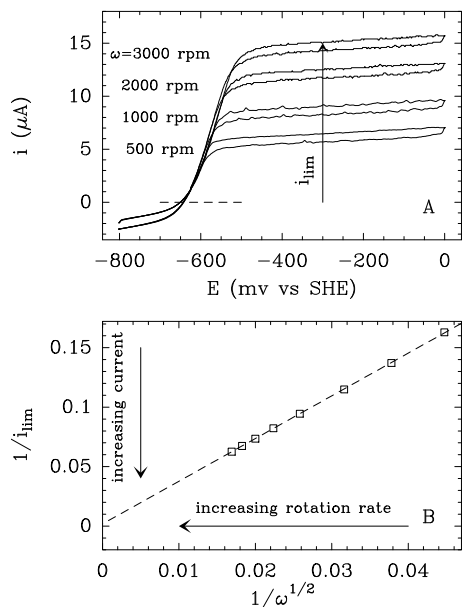


Figure 17: (A) Influence of electrode rotation rate ( $\omega$ , given in units Revolution Per Minute) on the catalytic current measured for hydrogen oxidation by *Allochromatium vinosum* NiFe hydrogenase adsorbed at a rotating graphite electrode. (B) Koutecky-Levich plot (eq. 31) showing small but non-zero intercept at infinite rotation rate, allowing one to estimate  $k_{\text{cat}}$ . 0.1 bar  $\text{H}_2$ ,  $\nu = 100\text{mV/s}$ ,  $T = 45^\circ\text{C}$ ,  $\text{pH} = 6.5$ . Adapted with permission from ref [73]. Copyright (1999) American Chemical Society.

published value  $E^{0'} \approx +20\text{mV}$  at  $25^\circ\text{C}$ ,  $\text{pH} 7$  ( $E^{0'} + RT/2F \ln([F]/[S]) = -46\text{mV}$ ). As a general way of things, provided the solution contains both the oxidized and reduced substrates, and that the adsorbed enzyme is able to catalyse both the oxidation and reduction reactions at significant rates, the value of the OCP is given by the Nernst equation and does not tell us anything about the enzyme. It only characterizes the substrate/product redox couple. In contrast, the value of the current on either side of the OCP and its dependence on electrode potential reveal the enzyme's intrinsic properties.

Catalytic electrochemistry offers several advantages with respect to conventional solution assays of the enzyme's activity.

- The temporal resolution of the activity is very high (the current can easily be sampled every 0.1s or faster), which is useful if the activity of the enzyme is evolving. For reasons which will become clear below, this makes it possible to study very easily the reaction of certain enzymes with their gaseous substrates or inhibitors ( $\text{CO}$ ,  $\text{H}_2$ , etc).
- In contrast to certain solution assays, anaerobicity is not required (at least on condition that the electrode potential is high enough that oxygen is not reduced on the electrode), which makes it possible to study the reaction of the enzyme with oxygen; this has proved very useful recently in the field of hydrogenase research [16, 54].
- Last, and most importantly, the electrode potential is a very useful control parameter, which influences the redox state of the enzyme and determines the driving force for the catalytic reaction and for certain redox-driven (in)activation processes. The dependence of activity on electrode potential can be very complex, and in some cases, efforts are still being made to make sense of the data in relation to the catalytic mechanism.

The magnitude and shape of the catalytic signal depend on a number of factors because catalysis involves many consecutive reactions or processes: transport by convection and diffusion of the substrate in solution towards the adsorbed enzyme, substrate diffusion *within* the enzyme,

its binding and transformation at the active site, product release and diffusion away from the enzyme, regeneration of the redox state of the active site upon intramolecular electron transfer (assuming there is a redox chain in the enzyme) and interfacial electron transfer between the electrode and a redox center that is exposed at the protein surface.

The overall turnover rate depends on the slowest of these steps, noting that changing the electrode potential changes the rates of the redox processes. This means that if one is interested in studying the catalytic mechanism, one should try to reach a situation where interfacial electron transfer and mass transport in solution do not limit the current. A good kinetic model will not include all steps (this would lead to indeterminateness), but only those which influence the turnover rate. Often the examination of the catalytic signal gives very useful information about which steps matter, as discussed below. Although kinetic models exist and are adapted to many different situations, they will not be described below and we shall only refer the reader to the primary literature. However, it is important to acknowledge that enzyme kinetics and electrochemistry are quantitative sciences, and that by looking at the data too superficially or qualitatively, one may miss important information or misinterpret the data.

## 7.2 Mass-transport controlled catalytic voltammetry

Figure 17A illustrates the voltammetry for hydrogen oxidation by *Allochromatium vinosum* NiFe hydrogenase adsorbed at a rotating disc electrode. In this experiment, the positive current at high potential is proportional to the rate of catalytic H<sub>2</sub> oxidation and the negative current results from proton reduction (H<sub>2</sub> evolution). The current tends to a limiting value at high potential, which increases dramatically as the electrode rotation rate  $\omega$  is raised [73]. This is because during turnover the concentration of hydrogen near the electrode decreases, the enzyme is able to consume H<sub>2</sub> faster than it is brought to the electrode by the convective motion of the solution. The greater the rotation rate, the more efficient the transport of hydrogen from the bulk solution towards the enzyme, and the greater the current (section 5.2). At infinite rotation rate, the catalytic current is finite: mass transport is no longer rate limiting, and the extrapolated current reveals the intrinsic efficiency of the enzyme. The Koutecky-Levich plot in fig 17B appears to follow:

$$\frac{1}{i_{\text{lim}}} \approx \frac{1}{nFA\Gamma \times (\text{turnover rate})} + \frac{\text{constant}}{\sqrt{\omega}} \quad (31)$$

The equation above emphasizes departure from mass-transport control at high  $\omega$  (compare to eq. (25)), but it is not rigorous (see [74] and section 2.3.1 in ref. [18]).

This limitation by mass transport is all the more influential that the enzyme has high activity, that the electrode coverage is high, and that the bulk concentration of substrate is small compared to the Michaelis constant (indeed, under saturating conditions, a small decrease of interfacial substrate concentration should have no effect on turnover rate).

The magnitude of the current is proportional to  $A\Gamma \times k_{\text{cat}}$ , and can give an estimate (sometimes only a lower estimate) of  $k_{\text{cat}}$ . Interestingly a study of hydrogenase showed that the turnover number of the enzyme is significantly higher than that observed in solution assays, using oxidizing dyes [73]; in the latter case, it becomes evident that turnover in solution assays is limited by electron transfer to the soluble electron partner, and that the electrode is a much faster electron

acceptor than the soluble dye.

### 7.3 Chronoamperometry to measure Michaelis and inhibition constants

In conventional biochemistry experiments, the rate of turnover is measured as a function of substrate concentration to determine the Michaelis-Menten parameters ( $k_{\text{cat}}$ , the maximal turnover rate, and  $K_{\text{m}}$ , the Michaelis constant):

$$\boxed{\text{turnover rate} = \frac{k_{\text{cat}}}{1 + \frac{K_{\text{m}}}{[\text{S}]}}} \quad (32)$$

The same parameters can be determined from chronoamperometric experiments looking at the substrate-concentration dependence of the current recorded at a fixed potential

$$i = nFA\Gamma \frac{k_{\text{cat}}}{1 + \frac{K_{\text{m}}}{[\text{S}]}} \quad (33)$$

In practice, this kind of measurement might be far from easy. (i) The limiting current is proportional to  $A\Gamma$ , the total amount of enzyme adsorbed, which can be determined (with a very relative accuracy) only when the electrode coverage is high enough for non-catalytic signals to be measured in the absence of substrate (eq. 28). (ii) The measurement of  $K_{\text{m}}$  can be performed without knowing the exact electroactive coverage. This requires however that the adsorbed film is stable enough as a function of time for the coverage to be constant when currents are measured with the same film in solutions of different substrate concentrations. Reference [75] describes methods for correcting the effect of film desorption. (iii) Last, eq. (33) does not take into account mass transport of substrate in solution; this is correct only if there is no depletion of substrate near the electrode. This should be checked for by looking at the rotation rate dependence of the current, or using the rotation rate dependence to extrapolate the current at infinite rotation rate.

Figure 18 shows the result of this simple chronoamperometric experiment, in a case where it is particularly informative: nitrate reduction by the molybdoenzyme *Rhodobacter sphaeroides* periplasmic nitrate reductase. Here, the effect of film desorption was corrected using a method proposed in ref [75]. The nitrate reduction rates (negative current) shown in the middle row were measured at two different electrode potentials. The top panels show the concentration of nitrate against time (each step corresponds to the injection in the electrochemical cell of a small amount of a concentrated stock solution of nitrate). The bottom panels show the steady state current at the end of each step plotted against nitrate concentration. At low potential (left column), the change in current simply follows Michaelis Menten kinetics, whereas under less reductive conditions (right column), high concentrations of nitrate inhibit the enzyme. This is particularly relevant because experiments aimed at trapping catalytic intermediates before they are characterized in spectroscopy are often carried out with very high concentrations of substrates; in the case of nitrate reductase, where moderately reducing conditions are needed to detect a Molybdenum(V) intermediate by EPR (the fully reduced Mo(IV) state is EPR-silent), fig. 18 demonstrates that these conditions favor the formation of an inactive enzyme, rather than a catalytic intermediate [76]. Solution assays with two electron donors having different reduction potentials fully supported these electrochemical results [76].

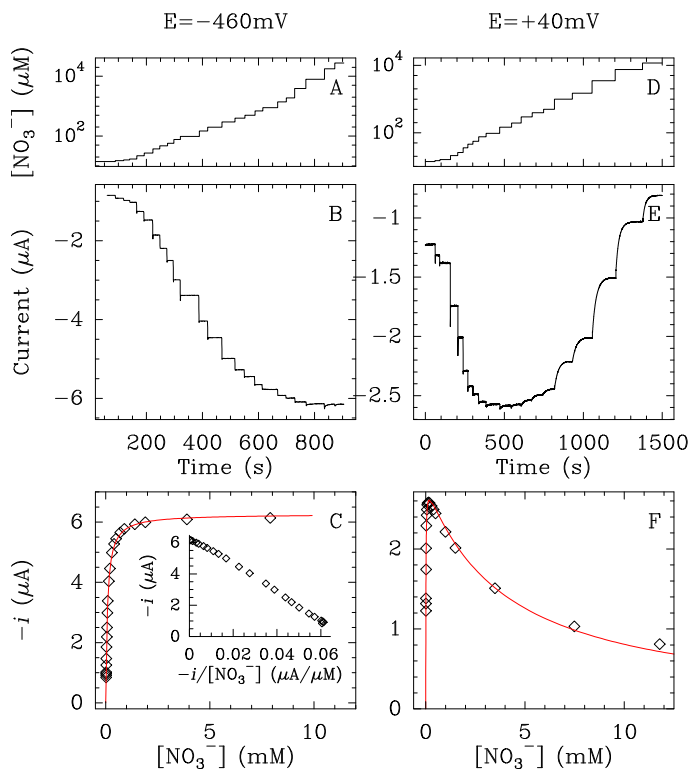


Figure 18: Dependence of the rate of nitrate reduction on nitrate concentration, with nitrate reductase adsorbed at a rotating disc electrode spun at a high rate. The left- and right-hand sides correspond to a redox poise at  $-460$  and  $+40$  mV vs SHE, respectively. Conditions: pH 6;  $25^\circ\text{C}$ ; 5 krpm. Panels A and D show the evolution of nitrate concentration against time, when the concentration is stepwise increased by adding aliquots of a stock solution of potassium nitrate (note the logarithmic Y scale). Panels B and E show the resulting change in catalytic current. Panels C and F show the catalytic current reached at the end of each step as a function of nitrate concentration. The fit of the data in C to the Michaelis-Menten returns the value of  $K_m \approx 85\mu\text{M}$ . The inset shows a Eadie-Hofstee plot [6]. The red line in panel F is the best fit to an equation accounting for substrate inhibition, with  $K_m = 10\mu\text{M}$  and  $K_i \approx 4\text{mM}$ . (C) American Chemical Society 2008. Reprinted with permission from ref [76]. Copyright (2010) American Chemical Society.

The high temporal resolution of the activity measurement is also useful for probing the reaction of redox enzymes with gaseous substrates and inhibitors. Many redox enzymes use, consume, or are inhibited by small molecules like  $\text{O}_2$ ,  $\text{CO}$ ,  $\text{N}_2$ ,  $\text{H}_2$ ,  $\text{NO}$  etc. The fact that these molecules tend to escape the solution and equilibrate with the gas phase above it makes certain experiments difficult. For example, to establish the competitive character of the inhibition of hydrogenase by  $\text{CO}$  by carrying out normal (solution) assays, one must measure the  $\text{H}_2$ -oxidation turnover rate as a function of the concentrations of  $\text{H}_2$  and  $\text{CO}$  dissolved in solution, but setting their concentrations precisely and maintaining them constant may be tricky and time-consuming. This problem is easily solved using electrochemistry, because it is possible to change the concentrations of dissolved gas in a controlled manner, and to simultaneously monitor the change in activity, as illustrated in fig. 19 [77].

Figure 19A shows in black the change in concentration of dissolved  $\text{H}_2$  against time that is obtained when, after having maintained an atmosphere of 1 bar of  $\text{H}_2$  until  $t=0$ , a small tube is suddenly plunged into the buffer and used to bubble argon. This flushes hydrogen away from the cell and its concentration decreases exponentially with time, with a time-constant which we denote by  $\tau_{\text{H}_2}$  [77]. The red curve in panel B shows the sigmoidal change in current for hydrogen

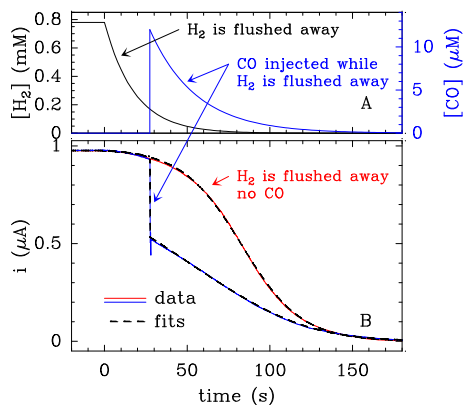


Figure 19: Hydrogen oxidation by WT *D. fructosovorans* NiFe hydrogenase adsorbed at a rotating disc electrode: measurement of the Michaelis constant relative to  $H_2$  and of the inhibition constant relative to CO. Panel A shows the change in hydrogen (black) and CO (blue) concentrations against time. The red line in panel B shows the change in current against time in the experiment where  $H_2$  is flushed away at  $t > 0$ . The blue line is the result of a similar experiment, but a solution saturated with CO was injected at  $t \approx 30$ s while the concentration of  $H_2$  was decreasing. The fits to eqs 34 and 35 are shown as dashed lines. Adapted with permission from ref [18]. Copyright (2008) American Chemical Society.

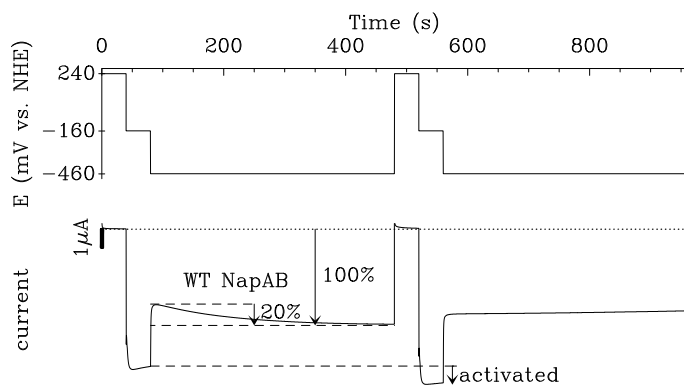


Figure 20: Chronoamperometric experiments demonstrating the irreversible reductive activation of NapAB. The top panel shows the sequence of potential steps which was applied to a film of as-prepared WT NapAB. Horizontal dotted lines are for  $i = 0$ .  $\omega = 5$ krpm, pH 6, 25°C. Adapted with permission from ref [78]. Copyright (2008) American Chemical Society.

oxidation by *D. fructosovorans* NiFe hydrogenase in the same experiment. The equation used to fit this data (black dashed line) is simply obtained by inserting into the Michaelis-Menten equation a time-dependent substrate concentration:  $[H_2](t) = [H_2]_0 \exp(-t/\tau_{H_2})$ .

$$i(t) = \frac{i_{\max}}{1 + \frac{K_m}{[H_2]} \exp(t/\tau_{H_2})} \quad (34)$$

In the second experiment, shown as a blue curve in Figure 19B, an aliquot of CO-saturated solution is injected at  $t \approx 30$ s while the hydrogen concentration is decreasing (blue line in panel A). In this experiment, the concentrations of both CO and  $H_2$  decrease with time, but the equation for the transient current is again simply obtained by using the rate equation that considers competitive inhibition by CO, in which we insert exponential decays of both  $H_2$  and CO:

$$i(t) = \frac{i_{\max}}{1 + \frac{K_m}{[H_2](t)} \left(1 + \frac{[CO](t)}{K_i}\right)} \quad (35)$$

The fit is shown as a dashed curve, and simultaneously determines  $K_m$  for  $H_2$  and  $K_i$  relative to CO, from an experiment that lasts no longer than a few of minutes! However, note that the sort of experiments shown in fig 19 cannot be very accurate; indeed, the concentrations varying exponentially with time, only the log (that is, the order of magnitude) of the values of  $K_m$  and  $K_i$  can be determined.

## 7.4 Chronoamperometry to resolve rapid changes in activity

Nitrate reductase is reversibly inactivated at high concentration of nitrate and moderate potential (figs 18 and 22F); in addition to that, it also irreversibly activates the first time it is reduced. This is clear from the chronoamperogram in Figure 20, which shows the response of a fresh film of periplasmic nitrate reductase immersed into a solution of nitrate when the potential is stepped as indicated in the upper panel. When the potential is poised at  $E = -160\text{mV}$  (at  $t = 40\text{s}$ ), the current is essentially constant. On the step to  $-460\text{mV}$ , at  $t = 80\text{s}$ , the activity first instantly decreases (the current becomes less negative) and then slowly increases before it stabilizes. This slow change in current demonstrates that the enzyme activates at low potential. The magnitude of the activation phase accounts for 20% of the current reached after activation. The instant decrease in activity when the potential is first stepped from  $-160$  to  $-460\text{mV}$  is not surprising considering the steady state profile in Figure 22D. When this sequence of potential steps is repeated with the same film of enzyme (from  $t = 480\text{s}$ , the activity detected at  $E = -160\text{mV}$  is greater than at the same potential in the first experiment, as indicated by the downward arrow, and no further activation occurs on the second step to  $-460\text{mV}$ , at  $t \approx 560\text{s}$ ). Therefore, the activation proceeds only once, on the first step to  $-460\text{mV}$ , and it is not reversed by taking back the enzyme to oxidizing conditions ( $+240\text{mV}$ ): it is irreversible.

This irreversible reductive activation cannot be detected in solution assays of the enzyme, because assaying the enzyme requires that it is reduced, and this reduction activates the sample. Therefore the enzyme molecules that are already active and those that require reductive activation are indistinguishable in solution assays. In contrast, the temporal resolution of the activity measurement in PFV is high enough that the activity can be measured while the enzyme is activating (fig 18). This is reminiscent of the “redox-cycling” experiment with *R. capsulatus* DMSO reductase : the enzyme has greater activity for DMS *oxidation* after it has been reduced [79]. Furthermore, the reductive activation of nitrate reductase is very relevant because its amplitude correlates with the concentration of a certain Mo(V) EPR signal (the so-called “high-g” signal) present in the sample before activation, demonstrating that, unlike all expectations, this signature arises from an inactive state which activates the first time the enzyme is reduced [78].

On a different note, chronoamperometry experiments with hydrogenase make it easy to characterize quantitatively the kinetics of inhibition by CO (and also  $\text{O}_2$ ). The experiment in fig. 21 consists in monitoring the  $\text{H}_2$ -oxidation current after the concentration of CO first suddenly increases when an aliquot of solution saturated with inhibitor is injected in the electrochemical cell, and then slowly returns to zero as the buffer is flushed by a stream of  $\text{H}_2$  (ref [77] and section 2.4.2 in ref [18]). The concentration of  $\text{H}_2$  is nearly constant, and the inhibitor concentration follows an exponential decay (panel A). The concentration of inhibitor need not be independently measured because its change against time is defined by the amount of inhibitor that is injected and by the time constant of the decay, which is determined by fitting the change in current [77]. If binding and/or release of the inhibitor is slow, the change in activity is delayed from the time of injection and the *rates* of inhibition can be measured [53].

In the case of the WT enzyme from *D. fructosovorans* (at  $40^\circ\text{C}$ ), the decrease in activity after CO injection is too fast to be resolved (black squares in fig. 21B). Also, the recovery of activity follows exactly the decrease in CO concentration as the latter is flushed away from the cell. In

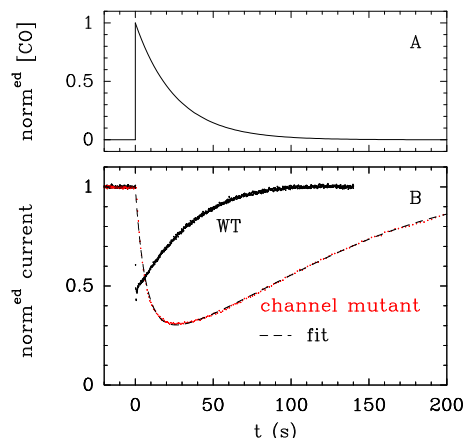


Figure 21: Inhibition by CO of H<sub>2</sub> oxidation by the native form of *D. fructosovorans* NiFe hydrogenase and a variant where a double mutation narrows the gas channel [53, 54]. Panel A: CO concentration against time. Panel B: the change in current against time for the WT enzyme (black) and the mutant (red). The modelling of these data directly gives the rates of diffusion along the channel [53, 54, 80]. The aliquot of solution saturated with CO was injected at  $t = 0$ . 1 bar H<sub>2</sub>,  $E = -160\text{mV}$ , pH7, 40°C, 3krpm. Reprinted with permission from ref [18]. Copyright (2008) American Chemical Society.

contrast, the red signal was obtained with a mutants of the enzyme, where amino acids whose side chains point inside the substrate channel connecting the active site to the solvent have been substituted [53]. Clearly, the binding and release of CO are much slower, suggesting that CO diffuses slowly within the mutant, to and from the active site. The data can be fit to the model in ref [80] to measure the rate constants corresponding to diffusion in the channel in either direction. Independent experiments based on solution assays of the isotope-exchange reaction confirmed the effects of the mutations on the rates of intramolecular diffusion, and proved that the difference between the two signals in fig. 21 is not an artifact resulting from the presence of the electrode [53].

Similar electrochemical experiments could be carried out to determine how the mutations of amino acids whose side chains point into the channel of hydrogenase affect the rates of binding and release of CO, O<sub>2</sub> and H<sub>2</sub>, and protein film voltammetry is now a unique tool for studying how the structure of gas channels affects intramolecular diffusion rates [53, 54, 81].

## 7.5 Determining the reduction potentials of an active site bound to substrate

Chronoamperometry experiments are usually easy to analyse, whereas understanding the profile of activity against potential sometimes demands effort. Figure 22 shows various catalytic voltammograms obtained with FrdAB, NapAB and hydrogenases adsorbed at rotating disk electrodes. We shall now discuss their *shape* (as opposed to merely their magnitude) and explain what can be learned about the enzyme from each signal.

We examine first succinate oxidation by *E. coli* fumarate reductase, FrdAB (Fig. 22A). Like all other data in this figure, this signal was obtained with the electrode rotating at a very high rate, so that mass transport was not influential. The background (capacitive) current is shown as a dotted line. At low electrode potential, the enzyme and its active site are reduced and unable to oxidize succinate, there is no activity and no Faradaic current. At very high potential the current tends to a limit (a plateau), *which is independent of electrode rotation rate*, and represents the maximal turnover rate when the enzyme is oxidized at a very high rate and therefore remains fully oxidized in the steady-state. In between the two, the activity increases when the electrode potential becomes high enough that the active site flavin becomes oxidized. The position of the inflection point of the main catalytic wave is a phenomenological parameter often called the “catalytic potential”. By

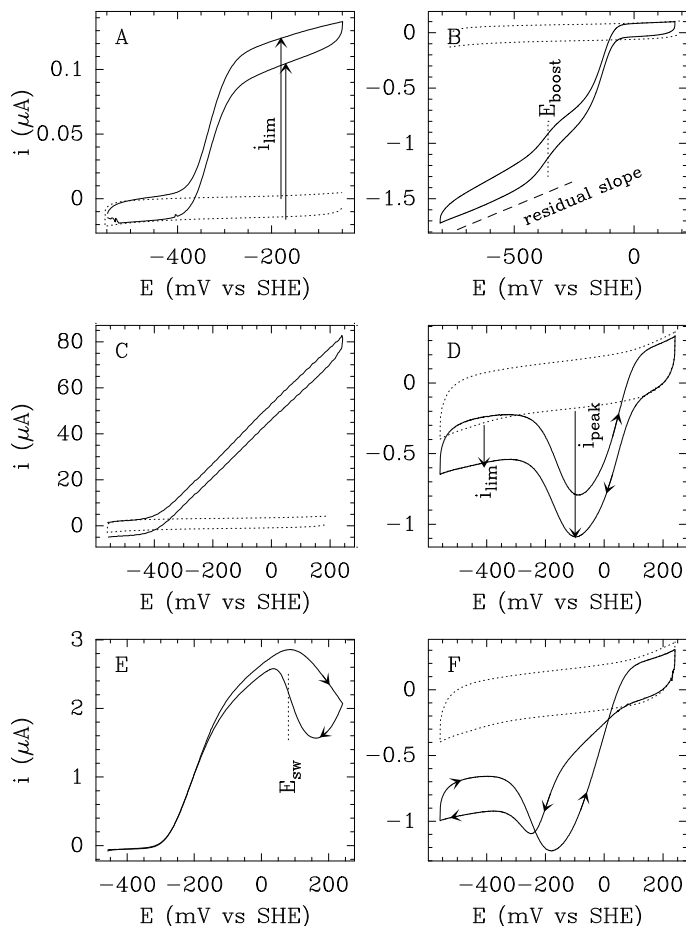


Figure 22: A small collection of cyclic voltammograms, obtained with various enzymes adsorbed at a rotating electrode spun at a high rate (so that substrate transport towards the electrode is fast). In most panels, the voltammogram plotted with a dotted line is a blank, recorded with no adsorbed enzyme: the contribution of the enzyme is obtained by subtracting this capacitive current. A: succinate oxidation by *E. coli* fumarate reductase  $\nu = 1\text{mV/s}$ ,  $\omega = 3\text{krpm}$ ,  $20^\circ\text{C}$ ,  $16\text{mM}$  succinate,  $\text{pH } 7.5$  [24] B: fumarate reduction by *E. coli* fumarate reductase. [82] C:  $\text{H}_2$ -oxidation by *A. vinosum* NiFe hydrogenase, at high temperature ( $60^\circ\text{C}$ ) and fast scan rate ( $\nu = 1\text{V/s}$ ),  $\omega = 2.5\text{krpm}$ ,  $1\text{bar}$   $\text{H}_2$ ,  $\text{pH } 7$  [83]. D: nitrate reduction by *R. sphaeroides* periplasmic nitrate reductase, at very low nitrate concentration ( $10\mu\text{M}$ )  $\nu = 20\text{mV/s}$ ,  $25^\circ\text{C}$ ,  $\text{pH } 6$  [84]. E:  $\text{H}_2$ -oxidation by *A. aeolicus* NiFe hydrogenase, at slow scan rate ( $\nu = 0.3\text{mV/s}$ ) [85]; compare with the signal in panel C. F: nitrate reduction by *R. sphaeroides* periplasmic nitrate reductase, at very high nitrate concentration ( $24\text{mM}$ )  $\nu = 20\text{mV/s}$ ,  $25^\circ\text{C}$ ,  $\text{pH } 6$  [76]; compare with the signal in panel D. Adapted with permission from refs [24,76,82–85], Copyright (2001–2010) American Chemical Society.

using a very simple kinetic model that uses the Nernst equation to relate the electrode potential to the redox state of the flavin, the *position* and precise *shape* of the voltammogram can be interpreted to determine the two reduction potentials of the active site flavin, under turnover conditions and in the presence of substrate. In contrast, in equilibrium titrations, the reduction potential of the active site flavin can only be measured in the absence of substrate, otherwise the enzyme would turnover and equilibrium could not be reached. In ref [24], voltammograms such as that in Panel A were used for determining the dependence of the reduction potential of the active site flavin on succinate concentration (shown in fig. 4) and  $\text{pH}$ , from which the affinity for succinate and  $\text{pK}_a$  of the flavin in its different redox states could be determined using equations such as eq. 9. These thermodynamic properties of the active site are relevant to the catalytic cycle, regarding the protonation and binding states of the FAD intermediates.

## 7.6 The effect of slow intramolecular electron transfer

The catalytic potential matches the reduction potential of the active site only if electron transfer between the electrode and the active site (both interfacial and intramolecular ET) is fast. If the enzyme has a chain of redox cofactors that relay electrons internally, and if one of the ET transfers along this chain is slow, then the catalytic potential may be shifted from the reduction potential of the active site, and approach the reduction potential of a relay [86]. This is indeed the prediction of models that take into account intramolecular ET along the chain [24]. How the catalytic potential compares to the reduction potentials of the relays may therefore inform on the rate of intramolecular ET.

For reasons that are not entirely clear yet, the shape of the catalytic wave may also have a particular feature at a potential that corresponds to one of the redox relays. For example the fumarate reductase discussed above has a series of 3 FeS clusters that connect the active site flavin to the solvent. The medial relay is a low potential [4Fe4S] cluster. The catalytic signal for fumarate reduction in figure 22B shows a first wave at the potential of the flavin, and a “boost” of activity at the potential of the [4Fe4S] cluster [82].

## 7.7 Slow interfacial electron transfer

In figures 22A and B, it also appears that the current does not reach a plateau at low potential, but instead it keeps increasing linearly. In some cases, this linear increase in current hides the underlying sigmoidal wave: this is so for example in figure 22C, which shows H<sub>2</sub> oxidation by a NiFe hydrogenase [83]. This is observed when (1) the rate of interfacial ET is not very fast compared to the enzyme’s turnover, *and* (2) not all enzymes are adsorbed in exactly the same orientation, which results in a distribution of interfacial ET rates.

The catalytic current corresponding to the assembly of enzymes molecules can be derived by averaging over the distribution of interfacial ET rate constants, and a linear change in current as a function of electrode potential at high driving force can indeed be predicted [83]. This results from the contribution of enzyme molecules having low  $k_0$  values which contribute only at high driving force. This effect, which blurs the signal and hides its interesting features, is all the more pronounced that the dispersion of orientation is wide and that interfacial ET ( $k_0$ ) is slow compared to the intrinsic turnover rate of the enzyme.

## 7.8 Slow substrate binding

Many redox enzymes exhibit complex activity profiles as a function of the electrode potential [9].

As a example, fig. 22D shows a catalytic voltammogram corresponding to the reduction of nitrate by *R. sphaeroides* nitrate reductase (NapAB) at very low nitrate concentration. The activity of the enzyme drops down (the current becomes less negative) when the electrode potential is decreased below  $-400\text{mV}$ , and it is recovered on the reverse scan.

One may first wonder whether this could be an artifact resulting *e.g.* from the reorientation of the enzyme on the electrode at low potential. However, the decrease in activity under very reducing conditions is also observed in solution assays carried out with reduced methyl viologen (MV): under conditions where the concentration of reduced MV greatly decreases during the

assay, so that the driving force for the reduction of nitrate decreases as a function of time, the activity measured in solution *increases* before MV is completely exhausted [87] (see also ref [88] for similar experiment with complex II). This mirrors the observation in fig 22D: starting from the low potential limit, the activity increases when the electrode potential is increased. This acceleration of turnover upon consumption of reduced MV was also made with the periplasmic nitrate reductase from *P. pantotrophus*, which exhibits the same voltammetry as in figure 22D [89] and *Rhodobacter capsulatus* periplasmic DMSO reductase [90], which belongs to the same family of molybdoenzymes. The membrane bound DMSO reductase from *E. coli* was the first molybdoenzyme for which a signature like that in as fig. 22D was observed [91]. Therefore, this peculiar relation between driving force and activity appears to be a common property of all reductases from the DMSO reductase family.

Although the concept of pH optima for enzyme activity is well established [6, 7], the possibility that activity of redox enzymes might be optimised within a narrow range of potential has been explored only recently. While pH optima give mechanistic information on protonation equilibria during catalysis, potential optima provide information on the roles played by different oxidation states of redox-active sites. Certain redox transitions may regulate electron flow to or from the active site. Or substrate binding or atom transfer may occur only when the active site is in a certain oxidation state. These relationships are difficult to observe by conventional techniques but can be revealed by protein film voltammetry, due to its ability to measure subtle changes in catalytic activity as the electrode potential is varied.

Considering the signal in fig. 22D, we now wonder what makes the activity drops under very reducing conditions. It has been proposed that the “switch off” results from the reduction of the [4Fe4S] cluster that relays electrons towards the active site [92]. However, there appears to be no correlation between the reduction potential of the [4Fe4S] cluster and the position of the low potential feature in the voltammogram [87]. It has also been proposed that the complex shape may result from the fact that catalysis can follow distinct routes, as substrate binding either precedes or follows the reduction of the active site, and the relative rates of the two reactions determine which track is used [91]. Indeed, changing the electrode potential changes the rate of reduction of the active site, which may make electron transfer faster or slower than substrate binding. When substrate binding to any redox state of the active site is taken into account in kinetic models, all sorts of complex waveshapes can indeed be predicted (see fig. 3 in ref [84]), and the signal in fig 22D can indeed be accurately predicted [84, 93].

## 7.9 Slow, redox-driven (in)activation

So far, we have only considered steady-state voltammograms, where the current depends on electrode potential but not on time, and the catalytic signal is therefore independent of scan rate and sweep direction. For example the switch on and off observed in fig 22D is observed at the same potential irrespective of whether the potential is scanned towards positive or negative potential, suggesting that whichever reaction triggers this modulation of activity is fast on the time scale of the voltammetric experiment (not necessarily so on the time scale of turnover).

Sometimes, the enzyme undergoes slow activation or inactivation processes as the potential is varied, and this results in a strong hysteresis: the magnitude of the current depends on time and

sample history, and the voltammogram depends on scan rate and direction (but this is not caused by the diffusion of the substrate, contrary to the situation discussed in section 5).

For example, NiFe hydrogenases reversibly deactivate under oxidizing conditions due to the over-oxidation of the active site. The enzyme has to be reduced (*e.g.* incubated with hydrogen or reduced MV) for the activity to be recovered. Figure 22E is a catalytic voltammogram showing H<sub>2</sub> oxidation with *A. aeolicus* NiFe hydrogenase. It is recorded essentially in the same conditions as in fig. 22C but for a slow scan rate (recording a whole catalytic voltammogram at this scan rate takes one hour). The activity of the enzyme, measured as a positive current, decreases above  $-200\text{mV}$ , and the activity is recovered as the potential is taken down. However, because the inactivation and reactivation are slow on the time scale of the voltammetry, the (in)activation reactions lag behind the change in electrode potential, resulting in a characteristic hysteresis. This inactivation was not observed in the electrochemical experiments depicted in fig. 22C because the scan rate was too fast: the enzyme was taken to high potential and back before the inactivation reaction could proceed [69]. One can also design experiments in which the electrode potential is held, and the slow change in current resulting from the (in)activation measured, to study the kinetics and mechanism of (in)activation [85, 94].

The shape of the signal in fig 22E is now fully understood, and a very important conclusion from the theoretical study is that the potential where the activity is recovered on the scan towards low potential is *not* the reduction potential of the inactive state [85] (a clear simple observation suggesting that it is not a thermodynamic quantity is indeed that its value is greatly dependent of scan rate over the entire range of accessible scan rates). This illustrates a pitfall of the qualitative interpretation of the voltammograms: an inflection point in a voltammogram cannot always be equated to a reduction potential.

The catalytic voltammogram in figure 22F may be the most complex reported to date. It shows how the nitrate reductase signal in fig 22D is deformed by a reversible (in)activation process that decreases the activity at high potential, and increases it under reducing conditions. The resulting strong hysteresis at high potential is only detected at a high concentration of nitrate (1M in panel E, compared to  $10\mu\text{M}$  in panel D). This is another manifestation of the inhibition of the enzyme by its substrate that we discussed in relation to figure 18, right column [76].

## 8 Softwares

An open-source program called SOAS [46] has been developed, first in the group of F Armstrong in Oxford and then in our lab in Marseilles, with the aim of analysing one-dimensional signals. It offers a large set of commands for handling voltammetric and chronoamperometric data. It is free of charge and can be compiled on computers running any flavor of Unix or Linux (including Mac OS X). Binary installers for MacOS X and Debian/Ubuntu distributions of Linux are available. See installation instructions on our web page at <http://bip.cnrs-mrs.fr/bip06/software.html>.

A new version of the program, QSOAS, is currently being developed in our group. It will eventually become available for all OS (including Windows). Check our web pages for updates.

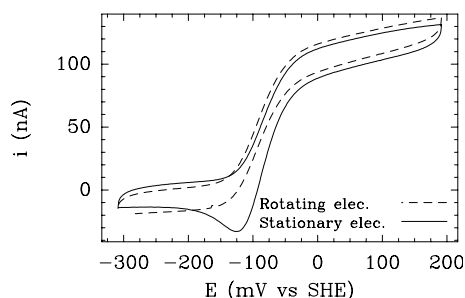


Figure 23: Effect of electrode rotation on the catalytic voltammetry of *E. coli* fumarate reductase (FrdAB) in a solution initially free of fumarate.  $[S] = 50\text{mM} \approx 200 \times K_m^{\text{succinate}}$ .

## 9 PFV Quiz

In fig. 23, we have plotted two voltammograms recorded with a film of *E. coli* fumarate reductase in contact with a solution containing only succinate at a concentration  $[S] = 50\text{mM}$  (approximately 200 times the Michaelis constant). The plain line corresponds to a stationary (non-rotating) electrode, whereas the dashed voltammogram was recorded with the electrode rotating at 3000rpm. (i) Why is the current at high potential rotation-rate independent in this case? (ii) Why are the shapes of the voltammograms different?

## Acknowledgements

I am very grateful to F. Armstrong (Oxford University, UK) for introducing me to this research field. Some of the data shown herein were obtained in his lab. I also thank him and A. K. Jones (formerly in Oxord, now at Arizona State University, USA) for proofreading an early version of this document. I thank Anne K. Jones, Harsh Pershad, Raoul Camba, James Mc Evoy and Lars J. C. Jeuken for kindly providing some of the data shown herein.

Our work in Marseilles is funded by the CNRS (mainly), Aix-Marseille Université, the Agence Nationale de la Recherche, the Region Provence-Alpes-Cote d'Azur and the city of Marseilles.

## A Appendices

### A.1 Notations and abbreviations

$\mathcal{A}$ : area under a pic (in units of VA).  $A$ : electrode surface.  $C$ : concentration of species, or capacitance (eq. 21), or coupling prefactor (eq. 15)..  $D$ : diffusion coefficient..  $\delta$ : peak width at half heighth.  $\eta$ : overpotential.  $E$ : electrode potential.  $E^0$ : reduction potential.  $E_p$ : peak potential. ET: electron transfer.  $F$ : Faraday constant.  $\Gamma$ : electroactive coverage.  $i$ : current.  $i_c$ : capacitive current.  $K_m$ : Michaelis constant.  $K_i$ : inhibition constant.  $k$ : rate constant.  $\lambda$ : reorganization energy.  $m$  number of protons. MV: methyl viologen.  $n$  number of electrons.  $\nu$ : scan rate.  $\nu_s$ : kinematic viscosity (eq. 25). OCP: open circuit potential.  $\omega$ : electrode rotation rate.  $R$ : gas constant. RDE: rotating disc electrode.  $T$ : temperature (in K).  $t$ : time.  $V$ : potential difference.  $\xi$ : extent of reaction.

## A.2 Derivation of eq. 9

We write the Nernst equation first for the alkaline couple Ox/Red, and then for both forms (protonated and deprotonated) of the redox couple:

$$E = E_{\text{alk}}^0 + \frac{RT}{nF} \ln \left( \frac{[\text{Ox}]}{[\text{Red}]} \right) \quad (36a)$$

$$E = E^{0'}([\text{H}^+]) + \frac{RT}{nF} \ln \left( \frac{[\text{Ox}] + [\text{OxH}]}{[\text{Red}] + [\text{RedH}]} \right) \quad (36b)$$

We rewrite eq. 36b as follows:

$$E = E^{0'}([\text{H}^+]) + \frac{RT}{nF} \ln \frac{[\text{Ox}] \left( 1 + \frac{[\text{H}^+]}{K_{\text{Ox}}} \right)}{[\text{Red}] \left( 1 + \frac{[\text{H}^+]}{K_{\text{Red}}} \right)} \quad (37a)$$

$$E = E^{0'}([\text{H}^+]) + \frac{RT}{nF} \ln \frac{[\text{Ox}]}{[\text{Red}]} + \frac{RT}{nF} \ln \frac{1 + \frac{[\text{H}^+]}{K_{\text{Ox}}}}{1 + \frac{[\text{H}^+]}{K_{\text{Red}}}} \quad (37b)$$

Equating eq. 37b and eq. 36a gives eq. 9:

$$E^{0'}([\text{H}^+]) = E_{\text{alk}}^0 + \frac{2.3RT}{nF} \log_{10} \left( \frac{1 + \frac{[\text{H}^+]}{K_{\text{Red}}}}{1 + \frac{[\text{H}^+]}{K_{\text{Ox}}}} \right) \quad (38)$$

Check that  $E^{0'}([\text{H}^+])$  tends to  $E_{\text{alk}}^0$  when  $[\text{H}^+]$  is small.

Using

$$E = E_{\text{acid}}^0 + \frac{RT}{nF} \ln \frac{[\text{OxH}]}{[\text{RedH}]} \quad (39)$$

instead of eq. 36a gives

$$E^{0'}([\text{H}^+]) = E_{\text{acid}}^0 + \frac{2.3RT}{nF} \log_{10} \left( \frac{1 + \frac{K_{\text{Red}}}{[\text{H}^+]}}{1 + \frac{K_{\text{Ox}}}{[\text{H}^+]}} \right) \quad (40)$$

Check that  $E^{0'}([\text{H}^+])$  tends to  $E_{\text{acid}}^0$  when  $[\text{H}^+]$  is large.

The relation between  $E_{\text{alk}}^0$  and  $E_{\text{acid}}^0$  is simply obtained by equating 36a and 39:

$$E_{\text{acid}}^0 = E_{\text{alk}}^0 + \frac{RT}{nF} \ln \frac{K_{\text{Ox}}}{K_{\text{Red}}} \quad (41)$$

Check that with  $pK_{\text{Ox}} < pK_{\text{Red}}$ ,  $E_{\text{acid}}^0 > E_{\text{alk}}^0$

## References

- [1] Bard, A. J.; Faulkner, L. R. *Electrochemical methods. Fundamental and applications. Third edition*; John Wiley & Sons, Inc.: 2004.
- [2] Compton, R. G.; Banks, C. E. *Understanding voltammetry*; Imperial College Press: 2011.

- [3] Newman, J.; Thomas-Alyea, K. E. *Electrochemical systems*; Wiley Interscience: 2004.
- [4] Levich, V. G. *Physical hydrodynamics*; Prentice-Hall, Inc.: 1962.
- [5] Savéant, J. M. *Elements of molecular and biomolecular electrochemistry*; John Wiley & sons, Inc.: 2006.
- [6] Cornish-Bowden, A. *Fundamental of Enzyme kinetics*; Portland Press.: 2004.
- [7] Laidler, K. J.; Bunting, P. S. *The Chemical Kinetics of Enzyme Action*; Clarendon Press. Oxford: 1973.
- [8] Armstrong, F. A.; Heering, H. A.; Hirst, J. *Chem. Soc. Rev.* **1997**, *26*, 169–179.
- [9] Elliott, S. J.; Léger, C.; Pershad, H. R.; Hirst, J.; Heffron, K.; Blasco, F.; Rothery, R.; Weiner, J.; Armstrong, F. A. *Biochim. Biophys. Acta* **2002**, *1555*, 54–59.
- [10] Léger, C.; Elliott, S. J.; Hoke, K. R.; Jeuken, L. J. C.; Jones, A. K.; Armstrong, F. A. *Biochemistry* **2003**, *42*, 8653–8662.
- [11] Murgida, D. H.; Hildebrandt, P. *Phys. Chem. Chem. Phys.* **2005**, *7*, 3773–3784.
- [12] Armstrong, F. A. *Curr. Op. Chem. Biol.* **2005**, *9*, 110–117.
- [13] Vincent, K. A.; Armstrong, F. A. *Inorg. Chem.* **2005**, *44*, 798–809.
- [14] Hirst, J. *Biochim. Biophys. Acta* **2006**, *1757*, 225–239.
- [15] Bernhardt, P. V. *Aust. J. Chem.* **2006**, *59*, 233–256.
- [16] Vincent, K. A.; Parkin, A.; Armstrong, F. A. *Chem. Rev.* **2007**, *107*, 4366–4413.
- [17] Cracknell, J. A.; Vincent, K. A.; Armstrong, F. A. *Chemical Reviews* **2008**, *108*, 2439–2461.
- [18] Léger, C.; Bertrand, P. *Chem. Rev.* **2008**, *108*, 2379–2438.
- [19] Jeuken, L. J. *Natural product reports* **2009**, *26*, 1234–1240.
- [20] Armstrong, F. A.; Belsey, N. A.; Cracknell, J. A.; Goldet, G.; Parkin, A.; Reisner, E.; Vincent, K. A.; Wait, A. F. *Chemical Society reviews* **2009**, *38*, 36–51.
- [21] Gates, A. J.; Kemp, G. L.; To, C. Y. Y.; Mann, J.; Marritt, S. J.; Mayes, A. G.; Richardson, D. J.; Butt, J. N. *Physical chemistry chemical physics : PCCP* **2011**, *13*, 7720–7731.
- [22] Lojou, E. *Electrochimica Acta* **2011**, in press.
- [23] Jeuken, L. C.; Camba, R.; Armstrong, F. A.; Canters, G. W. *J. Biol. Inorg. Chem.* **2002**, *7*, 94–100.
- [24] Léger, C.; Heffron, K.; Pershad, H. R.; Maklashina, E.; Luna-Chavez, C.; Cecchini, G.; Ackrell, B. A. C.; Armstrong, F. A. *Biochemistry* **2001**, *40*, 11234–11245.
- [25] Zu, Y.; Fee, J.; Hirst, J. *J. Am. Chem. Soc.* **2001**, *123*, 9906–9907.

- [26] Butt, J. N.; Sucheta, A.; Armstrong, F. A.; Breton, J.; Thomson, A. J.; Hatchikian, E. C. *J. Am. Chem. Soc.* **1993**, *115*, 1413–1421.
- [27] Butt, J. N.; Fawcett, S. E. J.; Breton, J.; Thomson, A. J.; Armstrong, F. A. *J. Am. Chem. Soc.* **1997**, *119*, 9729–9737.
- [28] Fawcett, S. E. J.; Davis, D.; Breton, J. L.; Thomson, A. J.; Armstrong, F. A. *Biochem. J.* **1998**, *335*, 357–368.
- [29] Gray, H. B.; Winkler, J. R. *Proceedings of the National Academy of Sciences of the United States of America* **2005**, *102*, 3534–3539.
- [30] Jeuken, L. J. C.; McEvoy, J. P.; Armstrong, F. A. *J. Phys. Chem. B* **2002**, *106*, 2304–2313.
- [31] Costentin, C.; Robert, M.; Savéant, J.-M. *Accounts of Chemical Research* **2010**, *43*, 1019–1029.
- [32] Anxolabéhère-Mallart, E.; Costentin, C.; Policar, C.; Robert, M.; Savéant, J.-M. M.; Teillout, A.-L. L. *Faraday discussions* **2011**, *148*, 83–95.
- [33] Wardman, P. *Journal of Physical and Chemical Reference Data* **1989**, *18*, 1637–1755.
- [34] Jeuken, L. J. C.; van Vliet, P.; Verbeet, M. P.; Camba, R.; McEvoy, J. P.; Armstrong, F. A.; Canters, G. W. *J. Am. Chem. Soc.* **2000**, *122*, 12186–12194.
- [35] Dutton, P. *Biochimica et Biophysica Acta (BBA) - Bioenergetics* **1971**, *226*, 63–80.
- [36] Leslie Dutton, P. [23] Redox potentiometry: Determination of midpoint potentials of oxidation-reduction components of biological electron-transfer systems. In , Vol. 54; Elsevier: 1978.
- [37] Tarasevich, M. R.; Yaropolov, A. I.; Bogdanovskaya, V. A.; Varfolomeev, S. D. *Journal of Electroanalytical Chemistry and Interfacial Electrochemistry* **1979**, *104*, 393–403.
- [38] Yaropolov, A. I.; Karyakin, A. A.; Varfolomeev, S. D.; Berezin, I. V. *Bioelectrochemistry and Bioenergetics* **1984**, *12*, 267–277.
- [39] Love, J. C.; Estroff, L. A.; Kriebel, J. K.; Nuzzo, R. G.; Whitesides, G. M. *Chemical Reviews* **2005**, *105*, 1103–1170.
- [40] Blanford, C.; Armstrong, F. *Journal of Solid State Electrochemistry* **2006**, *10*, 826–832.
- [41] Allongue, P.; Delamar, M.; Desbat, B.; Fagebaume, O.; Hitmi, R.; Pinson, J.; Savéant, J.-M. *Journal of the American Chemical Society* **1997**, *119*, 201–207.
- [42] Blanford, C. F.; Foster, C. E.; Heath, R. S.; Armstrong, F. A. *Faraday discussions* **2008**, *140*, 319–335.
- [43] Rudiger, O.; Abad, J. M.; Hatchikian, E. C.; Fernandez, V. M.; de Lacey, A. L. *J. Am. Chem. Soc.* **2005**, *127*, 16008–16009.

- [44] Alonso-Lomillo, M. A.; Rudiger, O.; Maroto-Valiente, A.; Velez, M.; Rodriguez-Ramos, I.; Munoz, F. J.; Fernandez, V. M.; de Lacey, A. L. *Nano Lett.* **2007**, *7*, 1603–1608.
- [45] Gutiérrez-Sánchez, C.; Olea, D.; Marques, M.; Fernández, V. M.; Pereira, I. A.; Vélez, M.; De Lacey, A. L. *Langmuir : the ACS journal of surfaces and colloids* **2011**, *27*, 6449–6457.
- [46] Fourmond, V.; Hoke, K.; Heering, H. A.; Baffert, C.; Leroux, F.; Bertrand, P.; Léger, C. *Bioelectrochem.* **2009**, *76*, 141–147.
- [47] Battistuzzi, G.; Borsari, M.; Sola, M.; Francia, F. *Biochemistry* **1997**, *36*, 16247.
- [48] Kudera, M.; Aitken, A.; Jiang, L.; Kaneko, S.; Hill, H. A. O.; Dobson, P. J.; Leigh, P. A.; McIntire, W. S. *J. Electroanal. Chem.* **2000**, *495*, 36–41.
- [49] Amatore, C.; Arbault, S.; Guille, M.; Lemaitre, F. *Chem. Rev.* **2008**, *108*, 2585–2621.
- [50] Chen, K.; Hirst, J.; Camba, R.; Bonagura, C. A.; Stout, C. D.; Burgess, B. K.; Armstrong, F. A. *Nature* **2000**, *405*, 814–817.
- [51] Dementin, S.; Belle, V.; Bertrand, P.; Guigliarelli, B.; Adryanczyk-Perrier, G.; Delacey, A.; Fernandez, V. M.; Rousset, M.; Léger, C. *J. Am. Chem. Soc.* **2006**, *128*, 5209–5218.
- [52] Léger, C.; Lederer, F.; Guigliarelli, B.; Bertrand, P. *J. Am. Chem. Soc.* **2006**, *128*, 180–187.
- [53] Leroux, F.; Dementin, S.; Burlat, B.; Cournac, L.; Volbeda, A.; Champ, S.; Martin, L.; Guigliarelli, B.; Bertrand, P.; Fontecilla-Camps, J.; Rousset, M.; Léger, C. *Proc. Nat. Acad. Sc. USA* **2008**, *105*, 11188–11193.
- [54] Liebgott, P.-P. *et al. Nature chemical biology* **2010**, *6*, 63–70.
- [55] McEvoy, J. P.; Armstrong, F. A. *Chem. Comm.* **1999**, 1635–1636.
- [56] Chobot, S. E.; Hernandez, H. H.; Drennan, C. L.; Elliott, S. J. *Angew. Chem. Int. Edit.* **2007**, *46*, 4145–4147.
- [57] Hagedoorn, P. L.; Driessen, M. C. P. F.; vandenBosch, M.; Landa, I.; Hagen, W. R. *FEBS Lett.* **1998**, *440*, 311–314.
- [58] Park, J. B.; Fan, C. L.; Hoffman, B. M.; Adams, M. W. W. *J. Biol. Chem.* **1991**, *266*, 19351–19356.
- [59] Brereton, P. S.; Verhagen, M. F. J. M.; Zhou, Z. H.; Adams, M. W. W. *Biochemistry* **1998**, *37*, 7351–7362.
- [60] Gilles de Pelichy, L. D.; Smith, E. T. *Biochemistry* **1999**, *38*, 7874.
- [61] Laviron, E. *J. Electroanal. Chem.* **1979**, *101*, 19–28.
- [62] Baymann, F.; Barlow, N. L.; Aubert, C.; Schoepp-Cothenet, B.; Leroy, G.; Armstrong, F. A. *FEBS Lett.* **2003**, *539*, 91–94.
- [63] Hirst, J.; Jameson, G. N. L.; Allen, J. W. A.; Armstrong, F. A. *J. Am. Chem. Soc.* **1998**, *120*, 11994–11999.

- [64] Hirst, J.; Duff, J. L. C.; Jameson, G. N. L.; Kemper, M. A.; Burgess, B. K.; Armstrong, F. A. *J. Am. Chem. Soc.* **1998**, *120*, 7085–7094.
- [65] Laviron, E. *J. Electroanal. Chem.* **1980**, *109*, 57–67.
- [66] Meunier-Prest, R.; Laviron, E. *J. Electroanal. Chem.* **1992**, *328*, 33–46.
- [67] Nicholls, D. G.; Ferguson, S. J. *Bioenergetic 3*; Academic Press: 2002.
- [68] Armstrong, F. A.; Camba, R.; Heering, H. A.; Hirst, J.; Jeuken, L. J. C.; Jones, A. K.; Léger, C.; McEvoy, J. P. *Faraday Discussions* **2001**, *116*, 191–204.
- [69] Limoges, B.; Savéant, J.-M. *J. Electroanal. Chem.* **2004**, *562*, 43–52.
- [70] Iverson, T. M.; Luna-Chavez, C.; Cecchini, G.; Rees, D. C. *Science* **1999**, *284*, 1961–1966.
- [71] Fontecilla-Camps, J. C.; Volbeda, A.; Cavazza, C.; Nicolet, Y. *Chem. Rev.* **2007**, *107*, 4273–4303.
- [72] Arnoux, P.; Sabaty, M.; Alric, J.; Frangioni, B.; Guigliarelli, B.; Adriano, J. M.; Pignol, D. *Nat. Struct. Mol. Biol.* **2003**, *10*, 928–934.
- [73] Pershad, H. R.; Duff, J. L. C.; Heering, H. A.; Duin, E. C.; Albracht, S. P. J.; Armstrong, F. A. *Biochemistry* **1999**, *38*, 8992–8999.
- [74] Heering, H. A.; Weiner, J. H.; Armstrong, F. A. *J. Am. Chem. Soc.* **1997**, *119*, 11628–11638.
- [75] Fourmond, V.; Lautier, T.; Baffert, C.; Leroux, F.; Liebgott, P.-P.; Dementin, S.; Rousset, M.; Arnoux, P.; Pignol, D.; Meynial-Salles, I.; Soucaille, P.; Bertrand, P.; Léger, C. *Anal. Chem.* **2009**, *81*, 2962–2968.
- [76] Fourmond, V.; Sabaty, M.; Arnoux, P.; Bertrand, P.; Pignol, D.; Léger, C. *The journal of physical chemistry. B* **2010**, *114*, 3341–3347.
- [77] Léger, C.; Dementin, S.; Bertrand, P.; Rousset, M.; Guigliarelli, B. *J. Am. Chem. Soc.* **2004**, *126*, 12162–12172.
- [78] Fourmond, V.; Burlat, B.; Dementin, S.; Arnoux, P.; Sabaty, M.; Boiry, S.; Guigliarelli, B.; Bertrand, P.; Pignol, D.; Léger, C. *J. Phys. Chem. B* **2008**, *112*, 15478–15486.
- [79] Bray, R. C.; Adams, B.; Smith, A. T.; Bennett, B.; Bailey, S. *Biochemistry* **2000**, *39*, 11258–11269.
- [80] Almeida, M. G.; Guigliarelli, B.; Bertrand, P.; Moura, J. J. G.; Moura, I.; Léger, C. *FEBS Letts.* **2007**, *581*, 284–288.
- [81] Lautier, T.; Ezanno, P.; Baffert, C.; Fourmond, V.; Cournac, L.; Fontecilla-Camps, J. C.; Soucaille, P.; Bertrand, P.; Meynial-Salles, I.; Léger, C. *Faraday discussions* **2011**, *148*, 385–407.
- [82] Hudson, J. M.; Heffron, K.; Kotlyar, V.; Sher, Y.; Maklashina, E.; Cecchini, G.; Armstrong, F. A. *J. Am. Chem. Soc.* **2005**, *127*, 6977–6989.

- [83] Léger, C.; Jones, A. K.; Albracht, S. P. J.; Armstrong, F. A. *J. Phys. Chem. B* **2002**, *106*, 13058–13063.
- [84] Bertrand, P.; Frangioni, B.; Dementin, S.; Sabaty, M.; Arnoux, P.; Guigliarelli, B.; Pignol, D.; Léger, C. *J. Phys. Chem. B* **2007**, *111*, 10300–10311.
- [85] Fourmond, V.; Infossi, P.; Giudici-Orticoni, M.-T. T.; Bertrand, P.; Léger, C. *Journal of the American Chemical Society* **2010**, *132*, 4848–4857.
- [86] Elliott, S. J.; McElhaney, A. E.; Feng, C.; Enemark, J. H.; Armstrong, F. A. *J. Am. Chem. Soc.* **2002**, *124*, 11612–11613.
- [87] Fourmond, V.; Burlat, B.; Dementin, S.; Sabaty, M.; Arnoux, P.; Etienne, E.; Guigliarelli, B.; Bertrand, P.; Pignol, D.; Léger, C. *Biochemistry* **2010**, *49*, 2424–2432.
- [88] Sucheta, A.; Ackrell, B. A. C.; Cochran, B.; Armstrong, F. A. *Nature* **1992**, *356*, 361–362.
- [89] Gates, A. J.; Richardson, D. J.; Butt, J. N. *The Biochemical journal* **2008**, *409*, 159–168.
- [90] Adams, B.; Smith, A. T.; Bailey, S.; McEwan, A. G.; Bray, R. C. *Biochemistry* **1999**, *38*, 8501–8511.
- [91] Heffron, K.; Léger, C.; Rothery, R. A.; Weiner, J. H.; Armstrong, F. A. *Biochemistry* **2001**, *40*, 3117–3126.
- [92] Anderson, L. J.; Richardson, D. J.; Butt, J. N. *Biochemistry* **2001**, *40*, 11294–11307.
- [93] Frangioni, B.; Arnoux, P.; Sabaty, M.; Pignol, D.; Bertrand, P.; Guigliarelli, B.; Léger, C. *J. Am. Chem. Soc.* **2004**, *126*, 1328–1329.
- [94] Jones, A. K.; Lamle, S. E.; Pershad, H. R.; Vincent, K. A.; Albracht, S. P. J.; Armstrong, F. A. *J. Am. Chem. Soc.* **2003**, *125*, 8505–8514.